UNIVERSITY OF SOUTHAMPTON

FACULTY OF ENGINEERING, SCIENCE AND MATHEMATICS
SCHOOL OF CHEMISTRY

Development of Superparamagnetic Particles for Analytical Pre-concentration

by

Luca Vescovo

Thesis for the Degree of Master of Philosophy

June 2011

UNIVERSITY OF SOUTHAMPTON

ABSTRACT

FACULTY OF ENGINEERING, SCIENCE AND MATHEMATICS
SCHOOL OF CHEMISTRY

Master of Philosophy

DEVELOPMENT OF SUPERPARAMAGNETIC NANO-PARTICLES FOR ANALYTICAL PRE-CONCENTRATION

by Luca Vescovo

The very low levels of trace heavy metals and organic pollutants in water can present difficulties for the analytical chemist that can often be overcome by employing a pre-concentration method to enrich the analyte. Adsorbants and reactive solid phase materials can be used to scavenge analytes from the solution and to isolate them from interfering species. In this work Fe_2O_3 superparamagnetic nano-particles were covered with a chemically modified mesoporous silica layer, able to uptake the target analyte. The solid phase, with attached analyte, can then be easily isolated from the sample solution by the application of an external magnetic field. Two different types of nano-sized particles were synthesised by modification of the silica by silanization. 3-aminopropyltriethoxysilane was reacted with the –OH groups present on the surface and in turn its $–NH_2$ groups were converted to dithiocarbamates. This type of particle was tested for copper extraction but was found to be unsuccessful due to the leakage of large quantities of iron into solution which competed with the analyte for the dithiocarbamate groups. Octa-decyltrichlorosilane was reacted with the silica surface to give a second type of particle specialised in collecting organic pollutants. Recoveries above 80% were obtained extracting polycyclic aromatic hydrocarbons and during a pilot experiment, 92% recovery of “tributyltin” was achieved.

Contents

Chapter 1 – Introduction

Chapter 2 – Synthesis and Characterization of Starting Materials

Chapter 3 – Dithiocarbamated Particles

Chapter 4 – C_{18} Modified Particles

Chapter 5 – Overall Conclusions

Declaration:

I declare that this thesis and the work described have not been submitted for any other degree, nor is it currently being submitted in candidature for any other degree.

The work is the result of my own investigations carried out at the University of Southampton.

Acknowledgements

I would like to thank Dr Alan Howard for his supervision and guidance during my time at the University of Southampton. Thanks also to my family and friends for their support.

Chapter 1

Introduction

1.1 Water Pollution and Trace Analysis

Life on earth depends on water. All biological systems evolve according to physical and chemical characteristics of the water they interact with. Since the last century human activities started to significantly influence this delicate equilibrium by the release of contaminants in the environment. When there are contaminants harmful to biological systems they are frequently labelled as *pollutants*. Usually pollutants are present in trace quantities and their measurement is very often a challenge for the analyst and a real scientific problem to solve.

IUPAC employs the term "*trace analysis*" for the measurement of any elements that have an average concentration less than 100 μg g^{-1} [1]. Modern techniques of sample preparation and analysis have significantly improved detection limits, and the new term "ultra-trace" is now used in the literature to cover the range from 1 μg ml^{-1} to 10 ng ml^{-1} or below [2]. However, a precise range for ultra-trace analysis is not defined and many non-systematic terms are in common usage in the literature [3]. The accurate identification and measurement of elements at low levels is so important that new legislation increasingly requires efforts to

decrease the concentrations in the environment to acceptable levels measurable at ultra-trace levels.

In a preliminary classification, pollutants can be divided in *inorganic* and *organic* [4].

1.1.1 Inorganics

Among the inorganics, *metal ions* are the most common class of pollutants. Some researchers focus on the so-called "heavy metals", even though there is no clear definition of this term [5]. Zn^{2+}, Cu^{2+}, Ni^{2+}, Cd^{2+} and Pb^{2+} are five of the most common pollutant metals released into the environment. In addition to the more obvious sources associated with metal mining and processing, even everyday activities such as road travel engine emissions, brakes and tyre wear result in release of metals to the environment [6].

A proportion of these pollutant metals remain in solution as cations and this form of the metals is thought to be more dangerous than others because they can be easily transported and are more readily available for uptake by plants, animals and humans. Heavy metal ions form complexes with carboxylic acid, amine and thiol groups present in proteins. These modified biological molecules lose their ability to function properly and malfunction or death of the cells may occur. When metals bind to these groups, they inactivate important enzyme systems and affect protein structure. This type of toxin may also cause the formation of radicals, dangerous chemicals that cause the oxidation of biological molecules [7]. Even though many heavy metals are essential to biological systems

(depending on their speciation and concentration) their presence can also be linked to fatal diseases, such as heart attacks, strokes and cancer. Many other diseases such as Alzheimer's disease, arthritis, diabetes, fatigue, memory loss, impotency, whilst not causing death, can affect the quality of life [8-9].

Arsenic is another widely distributed inorganic element that is well known for its toxic effects. In some parts of the world such as Bangladesh and in West Bengal, its high concentration in the aquatic environment arises from the local geology [9]. Arsenic can occur naturally in a variety of forms including arsenite and arsenate, the former of these species is significantly more toxic to humans than the latter [10]. Symptoms of chronic arsenic intoxication include changes in pigmentation of the skin and the appearance of hyperkeratosis of the palms of the hands and soles of the feet. A number of different types of cancer and congenital malformations may also occur [11].

1.1.2 Organics

Among the organic pollutants, *pesticides* are widely spread through the environment. Although there are benefits from the use of pesticides, there are also side effects such as potential toxicity to humans and other animals. Over 98% of sprayed insecticides and 95% of herbicides can be found far from where they are used [12]. As they are easily suspended in air, they are carried by wind to other areas. [13-16].

A second example of wide spread organic pollutants are the *polycyclic aromatic hydrocarbons* (PAHs). These compounds consist of fused aromatic rings. PAHs

can be found in oil, coal, and tar deposits, and are produced as by-products of fuel burning. Most of them have been identified as carcinogenic, mutagenic and/or teratogenic [17-18].

1.2 Pre-concentration

The concentration of an analyte prior its determination may be necessary for a number of different reasons:

- The concentration of the analyte may be too low for it to be directly measured using available instrumentation.
- The matrix of the sample may interfere.
- At low concentrations, losses of an analyte can occur during storage of the sample.
- Pre-concentration of the sample can ease its transport by reducing its mass or volume.

There are many ways that can be used to pre-concentrate an analyte in solution and the choice of method depends on its nature and the determination technique that is going to be used after the concentration [19]. Every pre-concentration approach presents its own advantages and disadvantages and methods are in a constant state of evolution.

One of the oldest and simplest ways to concentrate a solute is evaporation; a lot of energy is however used and the process is lengthy. During the process the matrix components also become concentrated potentially causing interference during the determination stage [20].

More sophisticated techniques had therefore to be developed that isolated the analyte from other matrix components during pre-concentration [21-22]. For instance, *electrochemical* methods have been developed. In this case the analyte is accumulated on the electrode (the pre-concentration step) and then by a faradic stripping process it can be redissolved in a smaller volume [23]. *Ion exchange* between two electrolytes can be realized to obtain separation/pre-concentration. Usually a polymeric or mineralic ion exchanger is involved in the process, a number of resins have been developed for both cations and anions [24]. *Foam flotation* is a common phenomenon based on differences in surface activity. Surface-activated material, which may be ionic, molecular, colloidal can be selectively adsorbed at the surface of bubbles from a foam present on the top of a solution [25]. *Synthetic membranes* have been also developed for separations for their endless applications [1, 26].

Whilst these techniques are valid and sophisticated, the most rapid, cost effective, with less manipulation and therefore popular are: *co-precipitation*, *solvent* and *solid phase extraction*.

1.2.1 Co-precipitation

During co-precipitation, metal ions are typically quantitatively precipitated from solution together with a carrier precipitate, isolated by filtration and released back by dissolution in strong acid (digestion phase). There are three main mechanisms by which the carrier and analytes can precipitate together. Analytes can be weakly *adsorbed* on the surface of the carrier, can be *included* in a lattice site of its crystalline structure or can be physically *occluded* during the formation of the crystal [20, 27]. Sometimes these mechanisms can occur simultaneously.

A very large number of applications have been reported and in this thesis it is possible to give just a few examples. For instance, arsenic and tin can be pre-concentrated by co-precipitation with a Ni-pyrrolidine dithiocarbamate. When the co-precipitates are analyzed by graphite-furnace-AAS, detection limits of 0.02 ng ml^{-1} for arsenic and and 0.04 ng ml^{-1} for tin, can be obtained [28]. Satisfactory co-precipitation was also obtained using bismuth(III) diethyl-dithiocarbamate to pre-concentrate lead, copper, cadmium, cobalt and nickel. These were recovered by dissolving the precipitate in 1 ml of concentrated HNO_3 and the analytes were determined by atomic absorption spectrometry [29]. Iron(III) and lead have been pre-concentrated using lanthanum phosphate as a co-precipitant, with the analytes then being determined by flame atomic absorption spectrometry. The method was capable of determining 2-300 μg L^{-1}. Synthetic zeolites were used as co-precipitating agents after dissolving them in nitric acid. When the aluminate-silicate solution is added to water sample containing trace metal ions and the pH of the solution is neutralized, an amorphous precipitate is formed containing the metals to be pre-concentrated. Gallium was extracted from environmental waters at pH 6-8. Yielding a detection limit of 0.8 μg L^{-1} [30]. Indium(III) hydroxide has been employed as a co-precipitation agent for the pre-concentration of heavy metals including Cd^{2+}, Co^{2+}, Cr^{3+}, Cu^{2+} and Pb^{2+} from water samples [31].

1.2.2 Solvent Extraction

This technique is based on the selective partitioning of the analyte or interferent between two immiscible phases and is widely used to separate trace organic compounds from aqueous solutions. Metals also can be extracted this way, after formation of suitable metal-complexes. When a phase containing a solute, S, is brought into contact with a second phase, the solute partitions itself between the two phases:

$$S_{phase\ 1} \leftrightarrows S_{phase\ 2}$$

The equilibrium constant K_D for this reaction is called *partition coefficient*. If K_D is sufficiently large, then the solute will move from phase 1 to phase 2. The solute will remain in phase 1 if the partition coefficient is sufficiently small. If a phase containing two solutes is brought into contact with a second phase and K_D is favourable for only one of the solutes, then a separation of the solutes may be possible. Usually an aqueous phase containing the analytes is present and a water-immiscible organic phase is used to extract them, exploiting its higher affinity for organic species; the separations that can be performed are simple, clean, rapid and convenient [32]. Typical solvents employed in this process are chloroform, dichloromethane and hexane. The choice of organic phase and aqueous phase pH is crucial to ensure that quantitative extraction of the analytes can be achieved. The two liquids are placed in a separatory funnel and shaken to increase the surface area between the phases. When the extraction is complete, the liquids are allowed to separate, with the denser phase settling to the bottom of the separatory funnel. This operation is more efficient using less volume of

solvent in more fractions than using it once in a larger volume. The disadvantages of the technique are the environmental impact cost, the issue of disposal of the solvent and low selectivity. The technique is also normally unsuitable for extraction from large water volumes and field use. The possible applications are never-ending and a few examples are shown.

Cadmium was extracted from river water into chloroform following a ligand substitution reaction with dithiozone [33]. Thorium was extracted using calyx[4]resorcinarene-hydroxamic acid. The recovery of thorium(IV) depended on the choice of solvent; a recovery of 11% was obtained when benzene was employed, but 100% was obtained with ethylacetate [34]. Himmi et al. studied the extraction into chloroform of Zn^{2+} as its 5-azidomethyl-8-hydroxyquinoline complex [35]. 5-methyl-1,3,4-thiodiazole-2-thiol chelation was used to remove Hg from acidified river water by extraction into benzene. Hg^{2+} was in an acidic solution and its complex was quantitatively extracted into benzene. The extracted complex was measured by HPLC [36].

1.2.3 Solid Phase Extraction

The separation ability of solid phase extraction is based on the relative affinities of desired and undesired solutes in a liquid for a solid with which the sample contacts. Impurities in the sample are either washed away while the analyte of interest is retained on the solid phase, or vice-versa. Analytes that are retained on the solid phase can then be eluted from the solid with an appropriate solvent. The solid phase is usually packed in a column or syringe-shaped cartridge,

allowing the operator to carry out a number of pre-concentrations simultaneously [37].

Solid phase extraction is more convenient than the older techniques for several reasons:

- It is fast and requires less manipulation.
- While the use of solvents is not totally avoided, the quantity used is less; this is good for the budget and the environment.
- It provides a high concentration factor. Factors of 1000 are often achieved.

A very large number of solid phase extractors have been produced. The adsorbent part can be a synthetic or a natural product [38].

Silica gel is a very important solid phase support due to the ease by which the silica surface can be modified using a large variety of silane reagents [39]. Silica has a high capacity and does not swell, is resistant to organic solvents and is thermally stable [40]. These characteristics make modified silica-based materials popular sorbents in solid phase extraction.

Hg^{2+}, for example, has been pre-concentrated from water using 4-(2-pyridylazo)-resorcinol anchored on nano-meter sized SiO_2 particles. Extracting 2 μg of Hg^{2+} from 100 ml of water the relative standard deviation was 2.45 % [41]. 8-hydroxyquinoline, one of the most popular chelating agents, has been successfully bound to a silica support by the Mannich reaction to give a material suitable for the extraction of metals such Cu^{2+}, Pb^{2+}, Cd^{2+}, Zn^{2+} and Mo^{6+} [42]. Perez reported that the collection of pesticide residues from lanolin was possible using C_{18} chains bound to silica. Lanolin was poured through a column of the C_{18} silica

and the pesticides were eluted with a mixture of acetonitrile/n-hexane. Recoveries ranged from 83 to 113% with a relative standard deviation < 20% [43].

1.3 Silica Particles

1.3.1 Stöber and Mesoporous Silica particles

The synthesis of uniformly sized spherical particles was introduced by Stöber et al. [44] in 1968 and was based on the work carried out earlier by Kolbe [45]. The method depends on the hydrolysis of alkyl silicates followed by condensation of silicic acid, $Si(OH)_4$, in the presence of ammonia and alcohol. Spherical silica particles of 50-2000 nm in diameter were obtained. Recently, Nagao et al. [46] made silica particles by hydrolysis of tetraethylorthosilicate, using three different basic catalysts: ammonia, methylamine and dimethylamine, and in the presence of acetic acid. They found that the size of their spherical particles depended on the type of catalyst employed and that maximum particle size was obtained using dimethylamine.

Mesoporous silicas have recently been developed, having uniform and controllable pore sizes around 1.5 nm in diameter [47]. Mesoporous silica can be synthesised in acid or base conditions by adding surfactant templates. The concentration of surfactant and other conditions play important roles in changing the pore size and morphology [48]. Hexagonal or cubic arrangements of parallel pores have been prepared. The formation of mesoporous silica using a pre-formed liquid crystalline phase as a template was introduced by Attard et al. [49] The method is based on the addition of tetramethoxysilane to ca. 50% (wt/wt)

aqueous solution of surfactant. A hexagonal mesoporous structure was obtained after gently removing the methanol side product.

1.3.2 The Mechanism of Silica Particle Formation

The first stage in the formation of many types of silica is the hydrolysis of a precursor, such as tetraethoxysilane or tetramethoxysilane, using a mineral acid or base. This step is followed by condensation, which eliminates alcohol and/or water and leads to the formation of siloxane bonds (Si-O-Si) [40], *Figure 1.1*.

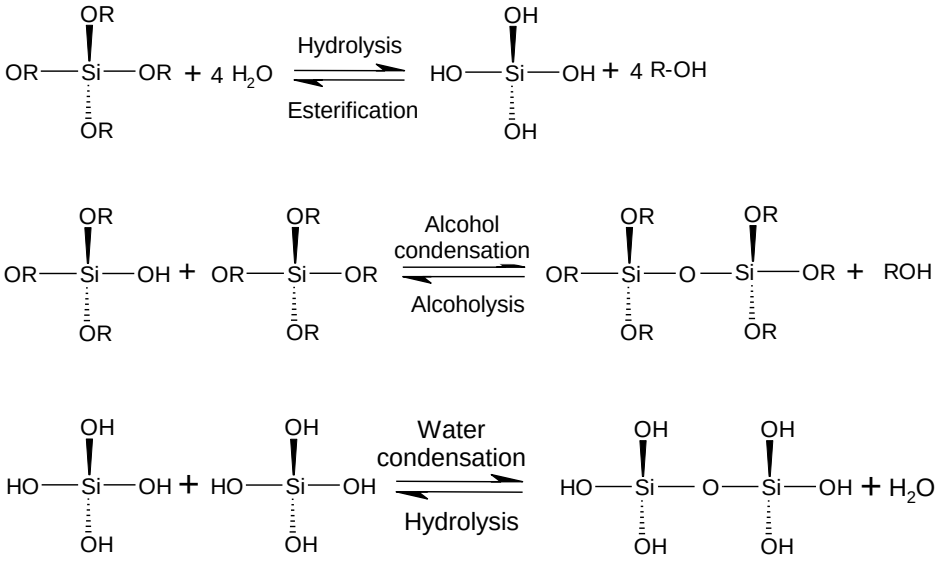

Figure 1.1 – Top: hydrolysis of alkoxysilane to form a silicic acid (monomer). Two monomers are condensed to form a dimer through the elimination of alcohol or water.

A number of researchers have studied how the final shape of the silica particles is reached. Green et al. [50] studied the kinetics leading to primary silica particles by

^{29}Si-NMR, ^{13}C-NMR and small angle X-ray scattering. They found that the first primary particles (nuclei) are thermodynamically controlled by monomer hydrolysis. Bogush and Zukoski [51] state, based on ^{29}Si NMR, that TEOS is hydrolyzed in the first few minutes,. Matsoukas et al. [40] reported the addition of a hydrolyzed monomer to the surface of a particle.

Iler [40] concluded that, under base conditions, the monomer reacts with hydroxyl ions, increasing the silicon coordination number from four to six. This new six coordinate molecule then reacts with another $Si(OH)_4$ molecule. Polymerization takes place when the monomers polymerize to form particles, which start to grow, and link into chains.

In basic media, hydroxyl ions attack the silicon atom (*Figure 1.2*) and through an S_N2 mechanism, the first alkoxide group is replaced with the hydroxyl group and further stages of hydrolysis develop [52].

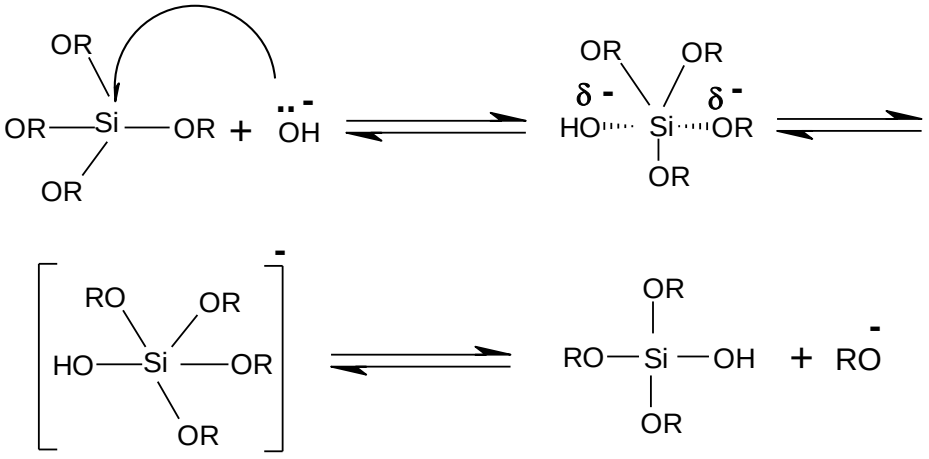

Figure 1.2 - The mechanism of hydrolysis of tetraethoxysilane in base media.

Khaskin [52] has shown by isotopic labelling experiments that the hydroxyl group on the hydrolysed silane is derived from the water, supporting the nucleophilic attacks on the silicon atom, (*Figure 1.3*).

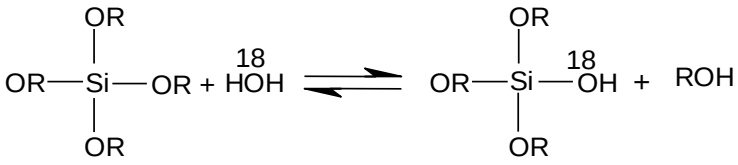

Figure 1.3 - Isotopic labelling of oxygen in silica hydrolysis.

Engelhardt et al. [53] used ^{29}Si NMR to study condensation products and found that at high pH, monomer, dimer, linear-trimer, cyclic-trimer, cyclic-tetramer (*Figure 1.4*) and higher order polymers were present with discrete primary particles being observed in the hydrolysis medium when turbidity began.

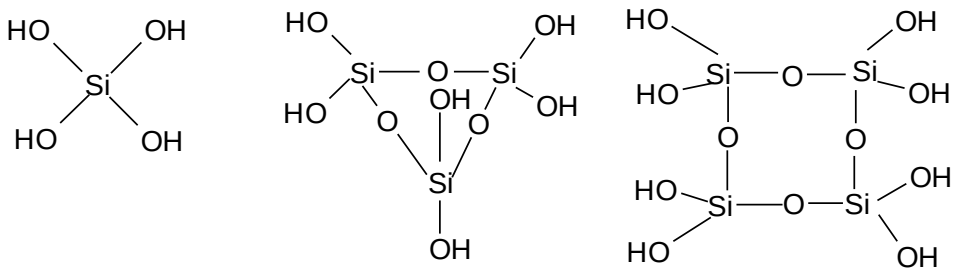

Figure 1.4 - Silicic acid (monomer) condenses to form cyclic-trimer and cyclic-tetramer species.

The formation of primary particles has been investigated in a number of different studies, the most reliable involving ^{29}Si NMR. These have shown that

condensation occurs by increasing the siloxane bonds and consequently reducing the number of hydroxyl groups by internal condensation [54] (*Figure 1.5*).

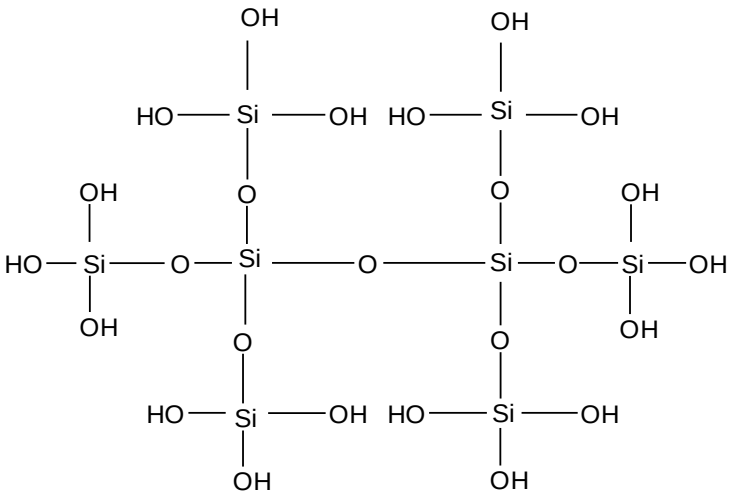

Figure 1.5 - Poly-condensation of monomer $Si(OH)_4$.

Two types of morphological catalysts are involved in the sol-gel process, acid and base catalysts, which yield primarily linear or random branched polymers respectively [55]. According to Iler [40] the polymerization process is different within three areas, pH less than 2, pH between 2 and 7 and pH above 7. At less than 2, the hydrolysis reaction is fast and complete and there is no formation of gel. At a pH between 2 and 7, the particles aggregate into a three-dimensional network by monomer and inter-cluster condensation of silanol groups, which causes the formation of a gel. Silica particles above pH 7 are considerably ionized, particle growth occurs without aggregation or gelation, and the size of particles increases by monomer addition. Subsequently the primary particles grow in size by dissolving and precipitating small particles onto large particles, which is known as the Ostwald ripening process.

Bogush et al. [51] found that once the primary particles had formed in the reaction mixture, they aggregated with other particles to form a larger particle. They supported their view by mathematical modelling, which indicated that, whilst the small particles repel each other, this force can be overcome by thermal forces, which allow the small particles to come together and bind [51]. Both mechanisms were considered by Harris et al. [56] to contribute to particle growth. Recently, Green et al. [50] found that, by addition of a soluble monomer to the primary particle, the size of the particle grows. They also found that the primary particle size depends on the solvent used; 8 nm particles are formed in ethanol, whilst 4 nm particles are formed in methanol.

1.4 Magnetic solid phase extractors

As described in *Section 1.2.3*, solid phase extraction became common in routine analysis due to its advantages compared with the previous techniques. Columns of silica-based extractors however still require a lot of manipulation, time and a moderate use of solvents.

In the last two decades magnetic carrier technology evolved into solid phase extraction. A distinct advantage of magnetic materials is that they can be easily isolated from sample solutions by the application of an external magnetic field.

The most convenient material for this purpose must have a size on the nanometre scale, and possess a large surface/volume ratio that allows it to be loaded with large quantities of analyte. Their surface must be adjustable in order to be selective for target compounds from complex environmental matrices. This

can be done by means of special functional ligands bound onto their surface, having affinities for the analyte present in solution. Furthermore it must be possible to disperse them very well in water and their magnetic properties occur only when an external magnet is applied.

Figure 1.6 shows how a typical routine extraction can be carried out using such particles. With a simple magnet the nano-particles can be recovered from their suspension together with the bound analyte. After displacing the analyte, it can be measured with a traditional technique such as FAA, HPLC, GC or UV-Vis spectroscopy. The volume of the matrix containing the analyte can be very large and this allows very high pre-concentration factors.

In the literature Fe_3O_4 (magnetite) has been commonly employed in magnetic solid phase extraction, but new materials are continuously being proposed. During this research Fe_2O_3 (maghemite) nano-particles were also used.

Magnetic carrier technology was first reported by Robinson [57] and became popular for bio-separations. Biological applications are made possible because nano-particles can be synthesised in a number of different sizes [58] which places them at dimensions that are smaller or comparable to those of cells, viruses, proteins or genes. This allowed them to interact with a biological target [59-61]. A few companies such as: Invitrogen, Micromer and Compel, have made commercially available several types of synthesised nano-particles, mainly employed in medical field. Some beads are pre-coupled with a biomolecule (ligand). The ligand can be an antibody, protein or antigen, DNA/RNA probe or any other molecule with an affinity for the desired target.

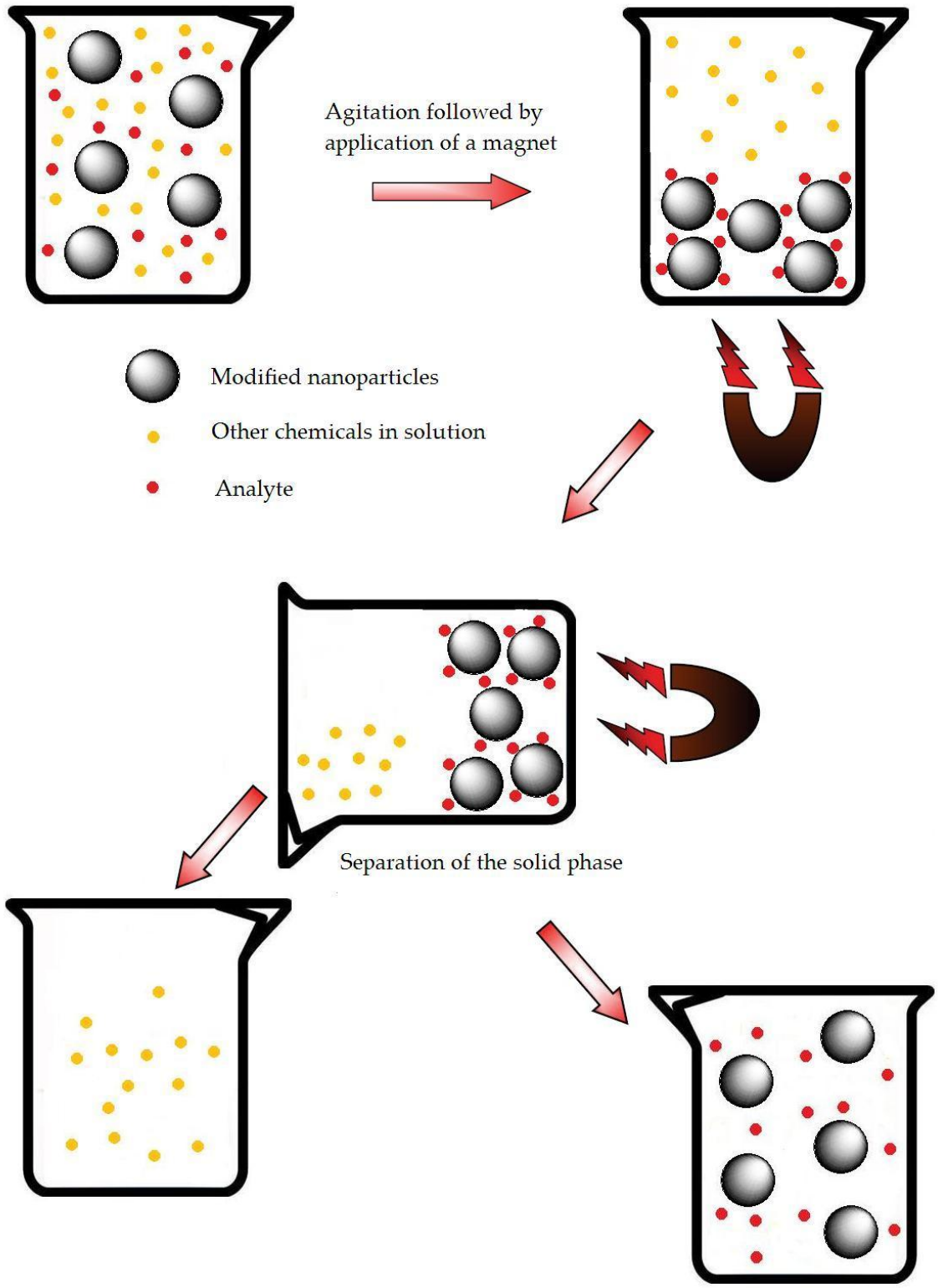

Figure 1.6 – Illustration of a typical pre-concentration using a magnetic solid phase.

Moving from the biological applications to pre-concentration, modified magnetic nano-particles have been reported giving good recoveries and pre-concentration factors, both for heavy metals and organic analytes. Huang and Hu, for example, modified Fe_3O_4 nano-particles with γ-mercaptopropyltrimethoxysilane for the fast and selective extraction of Cd, Cu, Hg and Pb [62]. Chuang et al. characterised a sort of "magnetic chitosan" and demonstrated its adsorbent properties [41].

There have been a number of reported syntheses and characterisations of modified nano-particles that are not good adsorbents, but are suitable supports for further modification. Shen et al., for example, modified magnetite with 3-aminopropyltriethoxysilane, that gives NH_2 groups. These are good collectors of certain species, but they can be more extensively exploited by attaching other collecting groups; depending on which analyte is to be pre-concentrated [63].

Sorbents can also be produced by the adsorption of ionic surfactants on the surface of the mineral oxides. Electrostatic attractive interactions between the head group of ionic surfactants and oppositely charged groups on the oxide result in the formation of mixed hemimicelle assemblies. The outer surface of the mixed hemimicelle is both hydrophobic and ionic, providing a two-fold mechanism for retention of analytes. The hemimicelle approach is more recent and gave good results for some organic compounds [64-65].

1.5 Magnetite and Maghemite Nano-particles

1.5.1 Introduction

Magnetite and maghemite nano-particles are *superparamagnetic*; that is they develop ferromagnetic order in the presence of a magnetic field. These nano-particles have found a number of practical applications in very different fields. It is possible; for example, to disperse them in water/solvent using surfactants to form a stable colloid-magnetic fluid (ferrofluid) [66]. Such magnetic liquids possess the properties of both liquid and solid magnetic materials and find applications in many fields. Space rocket engines, for example, had problems during the combustion of the fuel due to the microgravity. The issue was solved adding some magnetic liquid into the fuel and using magnets to control it [67].

1.5.2 Crystal structures

Among all iron oxide nano-particles, magnetite and maghemite (Fe_3O_4 and Fe_2O_3) present the most interesting properties due to their unique magnetic structures. Magnetite is found in abundance in nature and can also be readily synthesized [68].

Magnetite is a cubic mineral with an inverse spinel structure as shown in *Figure 1.7*. The inverse spinel structure of magnetite has the general formula $Fe_3O_4 = (Fe^{3+})_A\ (Fe^{3+}Fe^{2+})_B\ O_4$, where A and B symbolize the iron cations which are distributed at tetrahedral and octahedral interstitial sites, respectively. The Fe^{2+} ions and half the Fe^{3+} ions occupy octahedral sites; the other half of the Fe^{3+} ions occupies tetrahedral sites. As illustrated in *Figure 1.7*, a unit cell consists of four A and four B sites with a lattice constant of a = 0.8396 nm. The three-fold axis of rotation is along the diagonal [111] of the cubic cell. The inverse spinel structure of Fe_3O_4 consists of oxide ions in a face-centered cubic close packed arrangement

in which 1/3 of the tetrahedral interstices and 2/3 of the octahedral interstices coordinate with oxide ions [68-69].

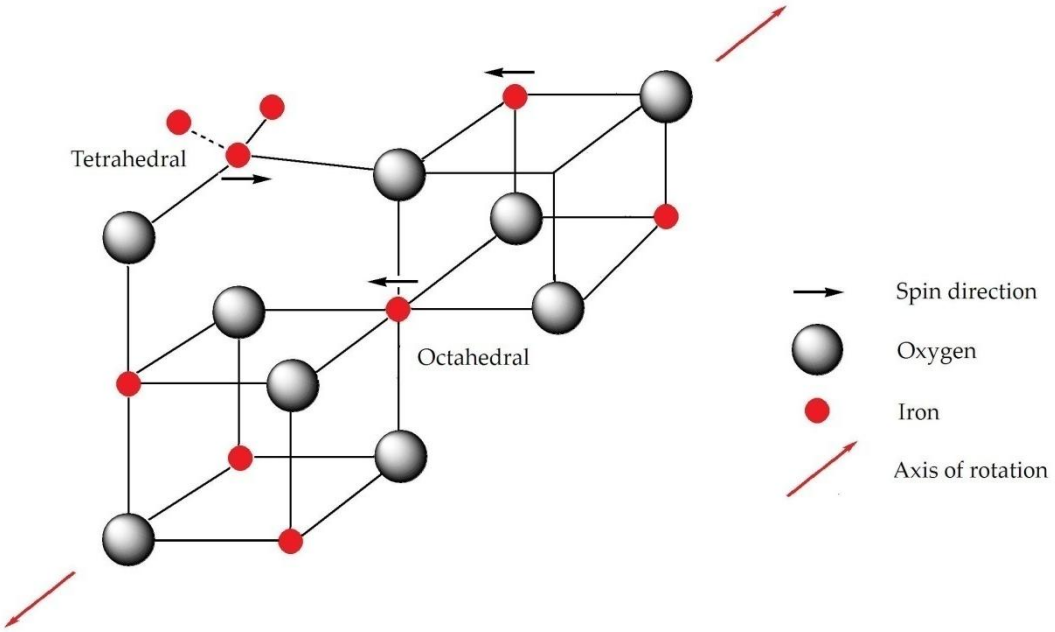

Figure 1.7 – Inverse spinel structure of magnetite.

The electron spins of the Fe^{3+} ions at the octahedral interstices are aligned antiparallel to those in tetrahedral interstices and hence no net magnetization is observed from these ions. The Fe^{2+} ions tend to align their spins parallel to those of Fe^{3+} ions in adjacent octahedral sites leading to a net magnetization.

Maghemite has a structure similar to that of magnetite but differs in that all or most of the Fe is in the trivalent state. Cation vacancies compensate for the oxidation of Fe^{2+}. Maghemite has a cubic unit cell with a constant a = 0.834 nm and each cell of maghemite contains 32 O^{2-} ions, 21 1/3 Fe^{3+} ions and 1/3 vacancies. Eight cations occupy tetrahedral sites and the remaining cations are randomly distributed over the octahedral sites. The vacancies are confined to the octahedral sites.

1.5.3 General discussion on the preparation

The synthesis of nano-composite materials of a controlled size has long been of scientific and technological interest [68]. The reduction of the size of iron oxide nano-particles leads to new and unusual magnetic properties of which superparamagnetism is the most important. Various synthetic methods have been reported in the literature for the preparation of these nano-particles which include ball milling [70], chemical precipitation [71], thermal decomposition [72] and sonochemical methods of preparation [73].

Chemical precipitation is the most common and successful approach. Synthesis of these materials through chemical precipitation includes:

1. Co-precipitation of Fe^{2+} and Fe^{3+},
2. Partial reduction of Fe^{3+}
3. Partial oxidation of Fe^{2+}, followed by co-precipitation.

Aqueous co-precipitation of Fe^{2+} and Fe^{3+} (at a ratio of 2:1) is commonly carried out in the presence of a base at pH 9-12, under anaerobic conditions [74]. Important factors that directly influence the nano-particle size and morphology are agitation time, reagent concentrations and pH of the solution. It has been demonstrated by Gur et al. [75] and Tegus et al. [76] that at the nano-scale it is possible to tune the physical, chemical, electronic and magnetic properties by modifying the nano-particle size and shape, which in turn is critically dependant on the experimental conditions.

The co-precipitation technique is the most versatile and convenient of all the above mentioned methods, not only for laboratory purposes but also potentially

on larger scale for industrial purposes [77]. Moreover, this technique is cost effective which further facilitates large scale synthesis. Even though the co-precipitation technique has been extensively used for the last few decades, the exact mechanisms controlling the final nano-particle size and distribution are still not clear. In this regard, an understanding of the process of nano-particles growth is a prerequisite to prepare nano-particles of the desired size, shape and properties. This is still subject of much research [76, 78].

The overall, deceptively simple, chemical reaction for the precipitation of nano-particles via co-precipitation from aqueous alkaline solutions is [68-69, 79-80].

$$\mathbf{Fe^{2+}(aq) + 2\ Fe^{3+}(aq) + 8\ OH^{-} \longrightarrow Fe_3O_4 + 4\ H_2O}$$

From the previous equation an initial molar ratio of Fe^{3+}: Fe^{2+} of 2 : 1 is required for the production of mixed oxidation state Fe_3O_4 small enough to behave as superparamagnetic nano-particles. It is known that Fe^{2+} can be readily oxidized in solution by dissolved or atmospheric molecular O_2, according to the following equation:

$$\mathbf{Fe^{2+}(aq) + \tfrac{1}{4}\ O_2 + \tfrac{1}{2}\ H_2O \longrightarrow Fe^{3+}(aq) + OH^{-}}$$

This in turn leads to favorable conditions for the production of extremely insoluble $Fe(OH)_3$:

$$\mathbf{Fe^{3+}(aq) + 3\ OH^{-} \longrightarrow Fe(OH)_3(s)}$$

Overall this oxidation can be represented as follows:

$$\mathbf{Fe_3O_4 + \tfrac{1}{4}\ O_2 + \tfrac{1}{2}\ H_2O \longrightarrow 3\ Fe(OH)_3(s)}$$

As a result of dissolved O_2, maghemite (γ-Fe_2O_3) can be formed:

$$\mathbf{Fe_3O_4 + \tfrac{1}{2}\, O_2 \longrightarrow 3\, \gamma\text{-}Fe_2O_3}$$

Usually when magnetite nano-particles are precipitated, the γ-Fe_2O_3 phase is likely to be present in the sample to some degree, depending on the amount of Fe^{2+} oxidation that has occurred. The formation of hematite (α-Fe_2O_3) is more difficult to obtain than that of the γ-Fe_2O_3 phase, which occurs only under thermal dehydration conditions [68-69].

Another prerequisite for the nano-particle formation during the synthesis is control of the pH of the aqueous solution [81]. A complete precipitation of Fe_3O_4 is expected between pH = 7.5 – 14, while maintaining a molar ratio of Fe^{3+} : Fe^{2+} = 2 : 1 [80]. Furthermore, rapid addition of the base with vigorous stirring of the aqueous suspension is essential, since it facilitates the formation of a large number of nuclei and prevents coagulation of particles. Synthesis under vigorous non-magnetic mechanical stirring is also important since it results in the formation of small particles by reducing their tendency to agglomerate [68-69].

1.5.4 Magnetic Properties of Iron Oxide Based Materials

Iron oxide materials such as Fe_3O_4 and Fe_2O_3 possess magnetic properties resulting in their response to an applied magnetic field. The magnetic properties of iron oxide nano-particles arise from electrons in motion [68-69]. Electrons spinning and revolving in orbits around atomic nuclei generate magnetic dipoles. The magnetic dipoles can either align in opposite directions, causing

cancellation, or can align in the same direction as the applied external magnetic field, producing bulk magnetism [67, 77, 82].

There are various forms of magnetism characteristic of iron oxide nano-particles that can arise depending on how their magnetic dipoles interact with each other. Any atom or ion of such nano-material that has one or more unpaired electrons is said to be paramagnetic [67-68]. This means that it, or another material in which it is found, will be attracted into a magnetic field. It should be emphasized that these materials will possess a stable magnetic moment only in the presence of an applied external magnetic field. In cases where paramagnetic atoms or ions are very close together and each one is strongly influenced by the orientation of the magnetic dipoles of its neighbours, more complicated forms of magnetism can arise. Examples of such magnetism may include ferromagnetism, antiferromagnetism and ferrimagnetism [68, 82].

Briefly, in ferromagnetism the interaction is such as to cause all magnetic dipoles to point in the same direction of the external magnetic field. Antiferromagnetism occurs when the nature of the interaction between neighbouring paramagnetic atoms or ions favours opposite orientation of their magnetic dipoles, thus causing partial cancellation. Ferrimagnetism is associated with materials in which the magnetic dipoles of the atoms on different sub-lattices are opposed. This happens when the sub-lattices of the material consists of different ions, such as metal ions with different valences [68].

1.5.5 Superparamagnetism

The problem with nano-sized Fe_3O_4 and Fe_2O_3 materials is that the individual nano-particles possess high surface energies, because of their large ratio of surface area to volume. For this reason, they have the tendency to interact with each other forming large aggregates in order to minimize their total surface energy. Moreover, because the Fe_3O_4 and Fe_2O_3 nano-particles are magnetic by nature, there is an additional contribution from strong, short range inter-particle magnetic dipole-dipole forces that further facilitates aggregate formation.

However, when the diameter of the particles is reduced to below a certain critical value (usually less than 35 nm), they lose their bulk ferromagnetism and are said to became superparamagnetic [79]. Superparamagnetism is associated with finite size and surface effects that dominate the magnetic behaviour of individual nano-particles. This phenomenon of superparamagnetism arises when the thermal energy within magnetic domains is sufficient to overcome the magnetic coupling forces between the nano-particles, causing their atomic magnetic dipoles to fluctuate randomly. When an external magnetic field is applied, the nano-particles acquire a certain magnetization, but because of the high thermal energy, the long range order is lost when the field is removed and the nano-particles have no remanent magnetization [67, 77, 82].

The superparamagnetic properties of Fe_3O_4 and Fe_2O_3 nano-particles are unusual because they represent single magnetic domains as illustrated in *Figure 1.8*. The ordering of electron spins characteristic of magnetic nano-particles leads to the formation of a region within a material which has uniform magnetization. The

nano-particles can become magnetized when the magnetic domains within the material are magnetized and aligned. This can be done by applying a moderate external magnetic field or by passing an electrical current through the bulk material, so that individual magnetic domains tend to align in the same direction as the external field. Some or all of the domains can be aligned. The more domains that are aligned the stronger the resultant magnetization of the material. When all of the domains are aligned, the material is said to be magnetically saturated.

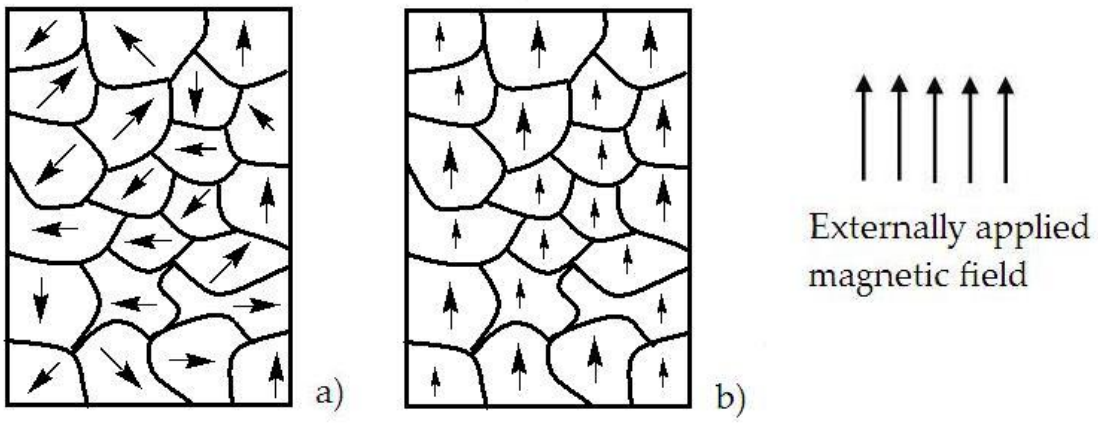

Figure 1.8 – Magnetic domains within superparamagnetic nano-particles.

1.5.6 The Ferrofluids and their Magnetic Properties

Due to their small size, superparamagnetic Fe_3O_4 and Fe_2O_3 nano-particles can be dispersed in an appropriate carrier liquid (aqueous or non-aqueous) to form a stable colloidal suspension called a ferrofluid or magnetic liquid. Such dispersions are stable for years, as distinct from the so-called magnetorheological fluids, which are dispersions of micron-sized particles [67]. Ferrofluids do not settle with time, not even when a magnetic field is applied. This stability can be

attributed to thermal energy that is sufficient to overcome the magnetic coupling forces between the nano-particles. Therefore, ferrofluids display the phenomenon of superparamagnetism. That is to say they exhibit relatively large saturation magnetization in the presence of moderate applied fields. This superparamagnetic behaviour is a feature that is in accordance with what should be expected from their finite nano-particles size. Magnetic properties of these nano-particles can be studied by means of a magnetization curve.

To induce magnetization, the nano-particle sample is exposed to an external magnetic field, H, and the magnetization, J, is recorded with a magnetometer. During the process, the magnetic material traces out a magnetization curve commonly known as a hysteresis loop similar to the one shown in *Figure 1.9*.

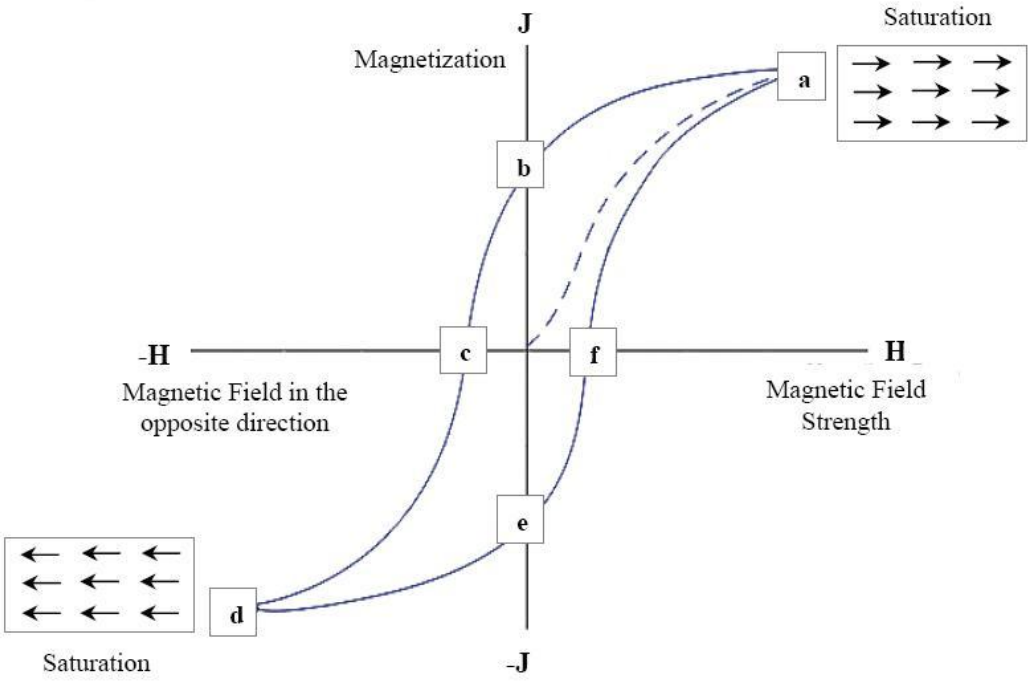

Figure 1.9 – Hysteresis associated to superparamagnetic materials.

As can be seen from *Figure 1.9*, with increasing magnetic field, the magnetization, **J**, of the material increases up to point **a** where magnetic saturation is reached. At this point, an additional increase in **H** will produce very little increase in **J**. Furthermore, at this point all the magnetic dipoles of materials are oriented parallel to one another. When the magnetic domains within the material are magnetized, the material will not relax back to zero, the curve will follow the path from **a** to **b**. The reason for this is that some of the magnetic domains remain aligned after the magnetic field is removed. The amount of magnetization that the material retains after the magnetic field is removed is called the remanance, **b** in the *Figure 1.9*. As the magnetic field is reversed, the curve follows the path from **b** to **c**. The force needed to remove the remanance, i.e. the residual magnetism, is called the coercivity of the material. Increasing the magnetic field further in the negative direction, the material will again become magnetically saturated (point **d**). Continuing applying the magnetic field but in the opposite direction, the curve will follow the path back to **a** and eventually complete the hysteresis loop. It is important to point out that zero coercivity and zero remanance on the magnetization curve indicate that the material is superparamagnetic in nature as indicated by the dotted line in *Figure 1.9*.

1.6 Aim of the Project

The aim of this project is to modify, with a silica layer, Fe_2O_3 nanoparticles, to which can be bound specific organic functional groups for use as magnetic solid-phase extractors. Maghemite is possibly a better choice with respect to magnetite for pre-concentration of cations in water, because it has been reported that under

certain conditions Fe^{2+} can be easily oxidized to Fe^{3+} and reduction of the cation analytes present in solution can occur [83-84]. Considering that in real water samples these are present in trace quantities, the possibility of reducing them is very dangerous, because they may not be collected by the chelators.

Therefore the specific objectives are:

1. Synthesis and characterization of magnetic silica particles.
2. Surface functionalization with aminosilane and conversion of its amino group in dithiocarbamate. Test this material as a magnetic extractor for metal ions.
3. Surface functionalization with octadecyltrichlorosilane and test these particles for the pre-concentration of some organic pollutants.

1.7 References

[1] Z. B. Alfassi, *Determination of Trace Elements*, VCH, New York, USA, **1994**.

[2] R. J. C. Brown, M. J. T. Milton, *TrAC Trends in Analytical Chemistry* **2005**, *24*, 266.

[3] J. Namiesnik, *Critical Reviews in Analytical Chemistry* **2002**, *32*, 271.

[4] M. C. Bruzzoniti, C. Sarzanini, E. Mentasti, *Journal of Chromatography A* **2000**, *902*, 289.

[5] J. H. Duffus, *Pure and Applied Chemisry* **2002**, *74*, 793.

[6] A. P. Davis, M. Shokouhian, S. Ni, *Chemosphere* **2001**, *44*, 997.

[7] S. K. Dhar, *Metal ions in biological systems; studies of some biochemical and environmental problems*, Plenum Press, New York,, **1973**.

[8] N. Cerulli, L. Campanella, R. Grossi, L. Politi, R. Scandurra, G. Soda, F. Gallo, S. Damiani, A. Alimonti, F. Petrucci, S. Caroli, *Journal of Trace Elements in Medicine and Biology* **2006**, *20*, 171.

[9] A. K. Singh, *Current Science* **2006**, *91*, 599.

[10] Y. Yuan, G. Marshall, C. Ferreccio, C. Steinmaus, J. Liaw, M. Bates, A. H. Smith, *Epidemiology* **2010**, *21*, 103.

[11] K. Jomova, Z. Jenisova, M. Feszterova, S. Baros, J. Liska, D. Hudecova, C. J. Rhodes, M. Valko, *Journal of Applied Toxicology* **2011**, *31*, 95.

[12] G. T. Miller, *Sustaining the earth : an integrated approach*, 6th ed., Brooks/Cole, Pacific Grove, CA, **2004**.

[13] R. Haque, V. H. Freed, American Chemical Society. Division of Pesticide Chemistry., *Environmental dynamics of pesticides*, Plenum Press, New York, **1975**.

[14] L. Maltby, *Aquatic macrophyte risk assessment for pesticides*, CRC Press, Boca Raton, FL.

[15] N. N. Ragsdale, R. E. Menzer, *Carcinogenicity and pesticides: principles, issues, and relationships*, American Chemical Society, Washington, DC, **1989**.

[16] B. R. Wilson, *Environmental problems; pesticides, thermal pollution & environmental synergisms*, Lippincott, Philadelphia,, **1968**.

[17] R. Anliker, *Anthropogenic compounds*, Springer-Verlag, Berlin ; New York, **1980**.

[18] P. E. T. Douben, *PAHs : an ecotoxicological perspective*, Wiley, Chichester, England ; Hoboken, NJ, USA, **2003**.

[19] M. L. P. da silva, J. G. Gameiro, *Revista Brasileira de Aplicações de Vàcuo* **2006**, *25*, 123.

[20] A. G. Howard, P. J. Statham, *Inorganic trace analysis : philosophy and practice*, Wiley, Chichester ; New York, **1993**.

[21] D. Atanassova, V. Stefanova, E. Russeva, *Talanta* **1998**, *47*, 1237.

[22] O. M. El Hussaini, N. M. Rice, *Hydrometallurgy* **2004**, *72*, 259.

[23] D. A. Ogaram, R. D. Snook, *Analyst* **1984**, *109*, 1597.

[24] Z. Fang, B. Welz, *Journal of Analytical Atomic Spectrometry* **1989**, *4*, 543.

[25] M. Caballero, R. Cela, J. A. Perez-Bustamante, *Talanta* **1990**, *37*, 275.

[26] Z. B. Alfassi, C. M. Wai, *Preconcentration techniques for trace elements*, CRC Press, Boca Raton, **1992**.

[27] T. L. Brown, H. E. LeMay, *Qualitative inorganic analysis*, Prentice-Hall, Englewood Cliffs, N.J., **1983**.

[28] Q. Zhang, H. Minami, S. Inoue, I. Atsuya, *Fresenius' Journal of Analytical Chemistry* **2001**, *370*, 860.

[29] H. Sato, J. Ueda, *Analytical Sciences* **2001**, *17*, 461.

[30] H. Minamisawa, S. Iizima, M. Minamisawa, S. Tanaka, N. Arai, M. Shibukawa, *Analytical Sciences* **2004**, *20*, 683.

[31] U. Sahin, E. Tokalioglu, E. Kartal, A. Ulgen, *Chemia Analityczna* **2005**, *50*, 529.

[32] D. C. Harris, *Quantitative chemical analysis*, 5th ed., W.H. Freeman, New York, **1999**.

[33] T. Shimizu, Y. Hiraoka, M. Kikuchi, N. Uehara, *Analytical Sciences* **2005**, *21*, 1.

[34] V. K. Jain, S. G. Pillai, R. A. Pandya, Y. K. Agrawal, P. S. Shrivastav, *Analytical Sciences* **2005**, *21*, 129.

[35] B. Himmi, B. Messnaoui, S. Kitane, A. Eddaif, A. Alaoui, A. Bouklouz, M. Soufiaoui, *Hydrometallurgy* **2008**, *93*, 39.

[36] S. Ichinoki, A. Ishizawa, M. Asano, Y. Fujii, *Journal of Liquid Chromatography & Related Technologies*, *33*, 793.

[37] J. S. Fritz, M. Macka, *Journal of Chromatography A* **2000**, *902*, 137.

[38] Y. Cai, G. Jiang, J. Liu, Q. Zhou, *Analytical Chemistry* **2003**, *75*, 2517.

[39] H. A. Mottola, J. R. Steinmetz, *Chemically modified surfaces: proceedings of the Fourth Symposium on Chemically Modified Surfaces,* New York, NY, USA, **1992**.

[40] R. K. Iler, *The Chemistry of Silica*, Wiley, New York, **1979**.

[41] Y. H. Zhai, X. J. Chang, Y. M. Cui, N. Lian, S. J. Lai, H. Zhen, Q. He, *Microchimica Acta* **2006**, *154*, 253.

[42] E. S. Yanovska, O. V. Glushchenko, V. I. Karmanov, O. Y. Kichkiruk, V. A. Tertykh, *Adsorption Science & Technology* **2006**, *24*, 229.

[43] A. Perez, G. Gonzalez, J. Gonzalez, H. Heinzen, *Journal of AOAC International*, *93*, 712.

[44] W. Stöber, A. Fink, E. Bohn, *Journal of Colloid and Interface Science* **1968**, *26*, 62.

[45] G. Kolbe, Ph.D. thesis, Friedrich-Schiller University (Jena. Germany), **1956**.

[46] D. Nagao, H. Osuzu, A. Yamada, E. Mine, Y. Kobayashi, M. Konno, *Journal of Colloid and Interface Science* **2004**, *279*, 143.

[47] C. T. Kresge, M. E. Leonowicz, W. J. Roth, J. C. Vartuli, J. S. Beck, *Nature* **1992**, *359*, 710.

[48] J. S. Beck, J. C. Vartuli, W. J. Roth, M. E. Leonowicz, C. T. Kresge, K. D. Schmitt, C. T. W. Chu, D. H. Olson, E. W. Sheppard, *Journal of the American Chemical Society* **1992**, *114*, 10834.

[49] G. S. Attard, J. C. Glyde, C. G. Goltner, *Nature* **1995**, *378*, 366.

[50] D. L. Green, S. Jayasundara, Y. F. Lam, M. T. Harris, *Journal of Non-Crystalline Solids* **2003**, *315*, 166.

[51] G. H. Bogush, I. Zukoski, C. F., *Journal of Colloid and Interface Science* **1991**, *142*, 1.

[52] I. G. Khaskin, *Dokl Akad Nauk, SSSR* **1952**, *85*, 129.

[53] V. Engelhardt, W. Altenburg, D. Hoebbel, D. Weiker, Z. Anorg, *Allgemeine Chemie* **1977**, *43*, 418.

[54] R. Harris, G. Knight, E. Hull, *Journal of the American Chemical Society* **1982**, *194*, 79.

[55] C. J. Brinker, G. Scherer, *Sol-Gel Science: The Physics and Chemistry of Sol-Gel Processing*, Academic Press, New York, **1990**.

[56] M. T. Harris, R. R. Brunson, C. H. Byers, *Journal of Non-Crystalline Solids* **1990**, *121*, 397.

[57] P. J. Robinson, P. Dunnill, M. D. Lilly, *Biotechnology and Bioengineering* **1973**, *15*, 603.

[58] S. Sun, H. Zeng, *Journal of the American Chemical Society* **2002**, *124*, 8204.

[59] Q. A. Pankhurst, J. Connolly, S. K. Jones, J. Dobson, *Journal of Physics D-Applied Physics* **2003**, *36*, R167.

[60] S. Mornet, S. Vasseur, F. Grasset, E. Duguet, *Journal of Materials Chemistry* **2004**, *14*, 2161.

[61] P.-C. Lin, M.-C. Tseng, A.-K. Su, Y.-J. Chen, C.-C. Lin, *Analytical Chemistry* **2007**, *79*, 3401.

[62] C. Huang, B. Hu, *Spectrochimica Acta Part B: Atomic Spectroscopy* **2008**, *63*, 437.

[63] X. C. Shen, X. Z. Fang, Y. H. Zhou, H. Liang, *Chemistry Letters* **2004**, *33*, 1468.

[64] J. Li, X. Zhao, Y. Shi, Y. Cai, S. Mou, G. Jiang, *Journal of Chromatography A* **2008**, *1180*, 24.

[65] X. L. Zhao, Y. L. Shi, Y. Q. Ca, S. F. Mou, *Environmental Science & Technology* **2008**, *42*, 1201.

[66] C. Scherer, A. M. F. Neto, *Brazilian Journal of Physics* **2005**, *35*, 718.

[67] B. D. Cullity, C. D. Graham, *Introduction to magnetic materials*, 2nd ed., IEEE/Wiley, Hoboken, N.J., **2009**.

[68] R. M. Cornell, U. Schwertmann, *The iron oxides : structure, properties, reactions, occurrences, and uses*, 2nd, completely rev. and extended ed., Wiley-VCH, Weinheim, **2003**.

[69] U. Schwertmann, R. M. Cornell, *Iron oxides in the laboratory: preparation and characterization*, 2nd completely rev. and extended ed., Wiley-VCH, Weinheim ; New York, **2000**.

[70] G. F. Goya, *Solid State Communications* **2004**, *130*, 783.

[71] M. Mikhaylova, D. K. Kim, N. Bobrysheva, M. Osmolowsky, V. Semenov, T. Tsakalakos, M. Muhammed, *Langmuir* **2004**, *20*, 2472.

[72] K. Woo, J. Hong, S. Choi, H.-W. Lee, J.-P. Ahn, C. S. Kim, S. W. Lee, *Chemistry of Materials* **2004**, *16*, 2814.

[73] R. Vijayakumar, Y. Koltypin, I. Felner, A. Gedanken, *Materials Science and Engineering a-Structural Materials Properties Microstructure and Processing* **2000**, *286*, 101.

[74] J.-P. Jolivet, C. Froidefond, A. Pottier, C. Chaneac, S. Cassaignon, E. Tronc, P. Euzen, *Journal of Materials Chemistry* **2004**, *14*, 3281.

[75] I. Gur, N. A. Fromer, M. L. Geier, A. P. Alivisatos, *Science* **2005**, *310*, 462.

[76] O. Tegus, E. Bruck, K. H. J. Buschow, F. R. de Boer, *Nature* **2002**, *415*, 150.

[77] J. P. Jakubovics, *Magnetism and magnetic materials*, Institute of Metals, London ; Brookfield, VT, USA, **1987**.

[78] C. N. R. Rao, A. Müller, A. K. Cheetham, *The chemistry of nanomaterials : synthesis, properties and applications in 2 volumes*, Wiley-VCH, Weinheim, **2004**.

[79] H. S. Nalwa, *Encyclopedia of nanoscience and nanotechnology*, American Scientific Publishers, Stevenson Ranch, Calif., **2004**.

[80] R. Massart, V. Cabuil, *Journal De Chimie Physique Et De Physico-Chimie Biologique* **1987**, *84*, 967.

[81] L. Vayssieres, C. Chaneac, E. Tronc, J. P. Jolivet, *Journal of Colloid and Interface Science* **1998**, *205*, 205.

[82] D. J. Craik, *Electricity, relativity, and magnetism : a unified text*, Wiley, Chichester ; New York, **1999**.

[83] A. F. White, M. L. Peterson, *Geochimica et Cosmochimica Acta* **1996**, *60*, 3799.

[84] C. J. Matocha, A. D. Karathanasis, S. Rakshit, K. M. Wagner, *Journal of Environmental Quality* **2005**, *34*, 1539.

Chapter 2

Synthesis and Characterization of Starting Materials

2.1 Introduction

Covering iron oxide nano-particles with silica is common practice [1] [2] to:

- Protect the magnetic core from acidic environments.
- Maintain dispersion of the particles.
- Exploit the silica surface by reacting its –OH groups.

How this coating is carried out can be crucial as different procedures result in different silica loadings and alter the surface that is available to host organic ligands [3] [4].

Several methods were evaluated for the coating of Fe_3O_4 nano-particles during the first months of this project. The quantity of silica was measured gravimetrically and the procedure leading to highest SiO_2 content was then adopted for the coating of Fe_2O_3 nano-particles, because they were considered more suitable (*Section 1.6*). The synthesis of mesoporous silica particles (containing no magnetic core) was also carried out for comparison.

During this project many materials have been synthesized and characterized. Every synthesis has been repeatedly carried out with small quantities of material

which were then mixed together to avoid small differences that could affect further experiments.

The notation adopted in this thesis will be of the form "$mSiO_2@Fe_2O_3$" representing a core of maghemite that has then been covered by SiO_2. "$mSiO_2$" is used to refer to mesoporous silica.

2.2 Materials

Deionised water was obtained using an Elga Option 4 system. Fe_3O_4 and Fe_2O_3 nano-particles (10 nm diameter (98%)), tetraethyl orthosilicate (TEOS, 98%) and 3-mercaptopropyltrimethoxysilane (95%) were obtained from Aldrich. Ammonia solution (d = 0.880 g/cm^3, 35% (w/v)), hydrochloric acid (36% (w/v) laboratory grade), sodium hydroxide pellets, glacial acetic acid (analytical grade) and sodium phosphates (monosodium and disodium) (98%) were purchased from Fisher Scientific. Dodecyltrimethylammonium bromide (98%), polyvinyl-pyrrolidone, carboxyethylsilanetriol, DL-valine (98%), ascorbic acid (99%) and ninhydrin were purchased from Sigma-Aldrich. Hexadecyltrimethylammonium chloride (25% in water) was purchased from Fluka. 25 mm glass microfiber filters (GF/C 1.2 μm) were purchased from Whatman. 3-aminopropyltriethoxysilane (98%) was obtained from Alfa Aesar.

2.3 Synthesis of $mSiO_2@Fe_3O_4$ particles.

In *Method 1* the Stöber process (described in *Section 1.3.1*) was carried out in the presence of commercial Fe_3O_4 particles. In all the other *Methods* the Fe_3O_4 particles

were pre-treated with a reagent that could possibly help build the silica layer and increase the quantity of silica in the product [5] [6] [7].

Methods

Method 1. Stöber process.

0.864 g of stored-wet Fe_3O_4 (3 g in 200 mL water) was placed in a 500 mL beaker and dispersed in 200 mL of methanol and 250 mL of ammonia solution (d = 0.880 g/cm^3). 5 mL of tetraethyl orthosilicate (TEOS) was added dropwise while the mixture was stirred and the reaction was left for 1.5 hours at room temperature. The particles were attracted towards the bottom by the application of a magnet and the liquid was poured away. The particles were dispersed in 200 mL of deionised water, stirred mechanically for a few seconds and then again isolated from the liquid by the use of a magnet. This operation was carried out three times with deionised water and three times with methanol, to clean the particles of excess reagents.

Method 2. Silica templated with hexadecyltrimethylammonium chloride.

3 g of stored-wet Fe_3O_4 (3 g in 200 mL water) was placed in a 2 L beaker and dispersed in 1.5 L of deionised water. 16 ml of hexadecyltrimethyl-ammonium chloride (C_{16}TAC) was added and left for 20 minutes under magnetic stirring, to allow the formation of the micelles. 30 ml of TEOS and then 20 ml of NH_4OH (d = 0.880 g/cm^3) were added slowly. The mixture was stirred for 1.5 hours at room temperature and the particles were cleaned as

described in *Method 1* with deionised water and methanol. In order to remove completely the surfactant from the pores, the sample was left in a furnace for 12 hours at 400 °C, being reached by increasing the temperature by 10 °C per minutes from 25 °C. The surfactant can also be removed by refluxing the particles for 2 hours in a solution containing ethanol, deionised water and glacial acetic acid. The first method was always adopted in this thesis.

Method 3. Via a 3-mercaptopropyltrimethoxysilane intermediate.

0.720 g of stored-wet Fe_3O_4 (3 g in 200 mL water) was placed in a 500 mL beaker, washed 3 times with ethanol (as described in *Method 1)* and dispersed in 150 mL of ethanol. 1.5 mL of 3-mercaptopropyltrimethoxysilane was added dropwise. The mixture was stirred for 2 hours at 70 °C. The Stöber process (M*ethod 1*) was then carried out on this sample, after which the particles were washed as described in M*ethod 1.*

Method 4. Via a polyvinylpyrrolidone (PVP) intermediate.

279 mg of PVP was placed in a 500 mL beaker and dispersed in 400 mL of deionised water. 0.720 g of stored-wet Fe_3O_4 was added. The mixture was stirred at room temperature overnight. The Stöber process (M*ethod 1*) was then carried out on this sample and the particles were washed as described in M*ethod 1.*

Method 5. Via a carboxyethylsilanetriol intermediate.

246 mg of carboxyethylsilanetriol was placed in a 500 mL beaker and dispersed in 300 mL of deionised water. 0.720 g of stored-wet Fe_3O_4 was added. The mixture was stirred at room temperature overnight. The Stöber process (*Method 1*) was then carried out on this sample, with the particles being washed as described in M*ethod 1.*

2.4 Synthesis of Mesoporous Silica Particles ($mSiO_2$)

Method

310 mL of deionised water, 90 mL of ethylene glycol, 0.120 g of NaOH and 1.68 g of dodecyltrimethylammonium bromide (C_{12}TAB) were transferred to a 3000 mL conical flask and mixed gently for 15 minutes. 1.8 mL of tetramethyl orthosilicate (TMOS) was added dropwise and the speed of the stirring was increased. The mixture was left stirring to complete the reaction at 20 °C for 8 hours. The white solid was isolated from the liquid by centrifugation and dispersed again in deionised water by sonication. This procedure was carried out five times to wash the solid from unreacted chemicals. The solid was left to dry in an oven at 50 °C overnight. The surfactant was removed by calcination at 650 °C for 12 hours in a furnace, gently ramping the temperature to 650 °C to preserve particle integrity.

2.5 Measurement of SiO_2 Content

The silica contents of the particles synthesized in *Section 2.3* were measured to evaluate the effectiveness of each synthetic approach.

Method

The SiO_2 content was assessed by gravimetry. First, an accurately weighed mass (ca. 200 mg) of $mSiO_2@Fe_3O_4$ was digested in 20 mL of *aqua regia*. The remaining SiO_2 was isolated from solution by filtration using pre-weighed 25 mm glass microfiber filters. The filter containing the silica was washed with deionised water to remove acid and remaining iron. The solid and the filter were dried at room temperature and then placed at 400 °C for 3 hours to remove all the water. They were weighed and the silica content was obtained by subtraction. The magnetic content was also obtained by calculation.

Results

Method	% SiO_2	% Fe_3O_4
1	58	42
2	**71**	29
3	31	69
4	58	42
5	47	53

Table 2.1 – SiO_2 content of $mSiO_2@Fe_3O_4$ particles.

Method 2 (silica templated with C_{16}TAC) gave the highest SiO_2 content and was used for the rest of the project.

2.6 $mSiO_2@Fe_2O_3$ Particles

$mSiO_2@Fe_2O_3$ particles were synthesised using *Method 2* on commercial Fe_2O_3 nano-particles. The silica content of this new material was evaluated (*Section 2.5*) and 68% of SiO_2 was found. The change of magnetic core did not affect the quantity of silica on the nano-particles and this material was used for the rest of this thesis. The following *Sections* describe its characterization.

2.6.1 Fourier Transform Infrared Spectroscopy

Method

The synthesized particles were characterized by FT-IR spectroscopy, using a Nicolet 380 Smart Orbit spectrometer. This type of instrument allowed the sample to be studied directly, without compacting it within KBr pellets. Transmission mode was employed (32 scans per sample).

Results

Figure 2.1a shows the FT-IR spectrum of commercial Fe_2O_3 particles without any surface modification. The peak at 567 cm^{-1} is attributed to Fe-O stretching vibrations, while the rest of the spectrum shows no other relevant peaks, not even an O-H stretching vibration peak due to physisorbed water in the range 3200-3600 cm^{-1}. This wide peak can appear depending on the synthetic method used, the time elapsed from the synthesis and the humidity of the storage environment. *Figure 2.1b* shows the spectrum for the $mSiO_2@Fe_2O_3$. The silica modification was attributed to the peaks at 1060, 800 and 440 cm^{-1}, due to Si-O stretching vibrations. The Fe-O peak still remains at 567 cm^{-1}. The use of the

furnace to remove the surfactant had completely removed the physisorbed water and its peaks in the range 3200-3600 cm^{-1} were not present.

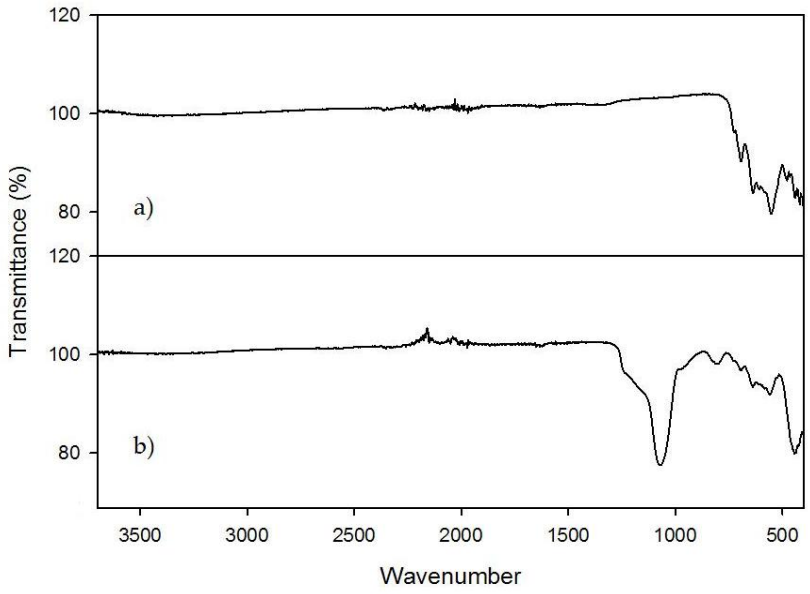

Figure 2.1 – a) FT-IR spectrum of Fe_2O_3 and b) $mSiO_2@Fe_2O_3$.

2.6.2 BET

Method

Surface area was calculated from nitrogen (77 °K) adsorption data using the approach described by Brunauer, Emmett and Teller (BET) [8]. Measurements were carried out using a Quantachrome NOVA 3000 automated gas sorption system with NOVA software (version 1.11). The sample was transferred to a pre-weighed tube. The tube was re-weighed and then degassed overnight at 150 °C. The tube was left to cool to room temperature, and then weighed. The tube was placed in the NOVA 3000 instrument and the surface area was determined from a multipoint BET plot of the adsorption data.

Results

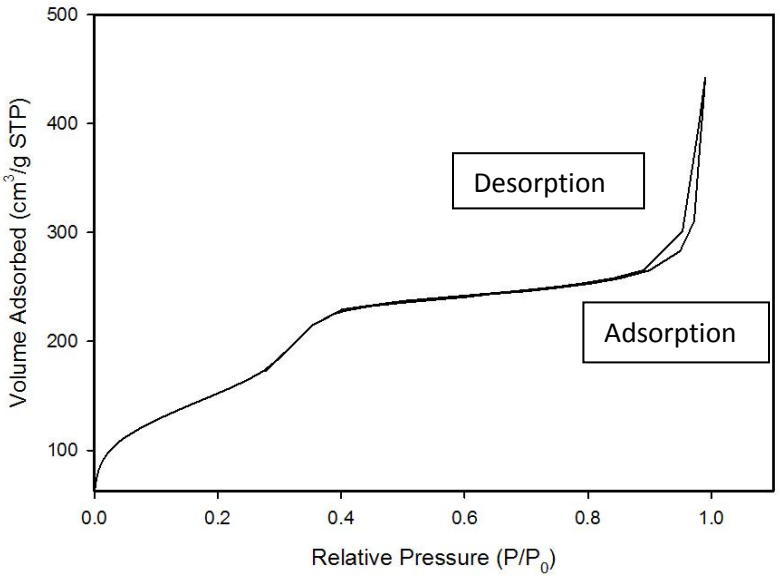

a)

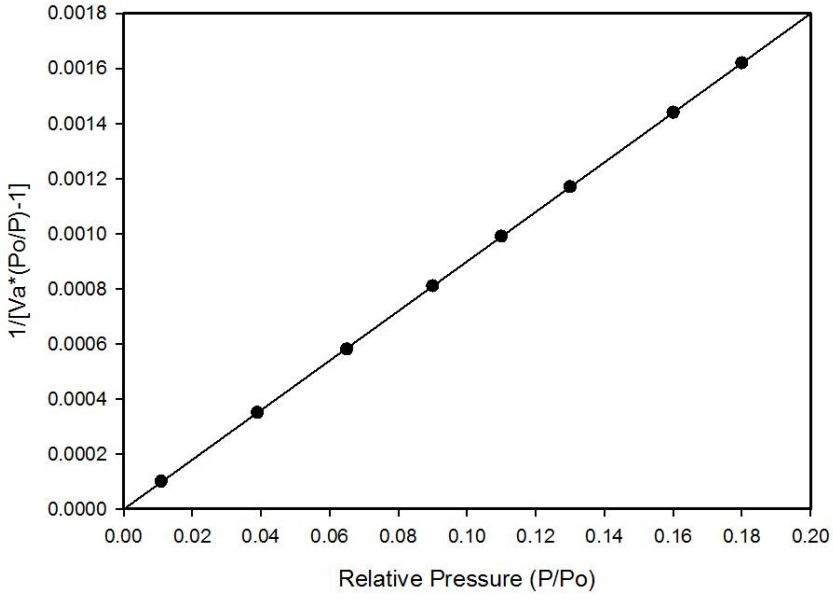

b)

Figure 2.2 – a) N_2 adsorption-desorption isotherms of $mSiO_2@Fe_2O_3$. b) Corresponding BET plot.

Figure 2.2a shows the adsorption-desorption isotherms. A hysteresis loop is visible, behavior typical of mesoporous (>20 Å) and macroporous (>500 Å) materials and corresponding to cylindrical pores. In general a wide hysteresis loop indicates a broad pore size distribution. *Figure 2.2b* shows the BET plot and *Table 2.2* the obtained results.

BET multipoint surface area (m^2g^{-1})	460
Total pore volume (cm^3g^{-1})	0.6835
Average pore diameter (Å)	109

Table 2.2 – BET results.

The average pore diameter of the $mSiO_2@Fe_2O_3$ indicates mesoporosity. Surface areas of Fe_2O_3 nano-particles typically range from 8 to 130 m^2g^{-1} and surface areas of Fe_3O_4 from 4 to 100 m^2g^{-1}, depending on the synthetic method [9]. The surface area available on the $mSiO_2@Fe_2O_3$ is therefore four times greater than that of the iron oxides.

2.6.3 Thermogravimetric Analysis

Method

Thermogravimetric analysis (TGA) was carried out using a Perkin-Elmer TGS-2 instrument attached to a Perkin-Elmer Datastation-3700 and a System 4 thermal analysis microprocessor. Approximately 10 mg of the sample was analyzed using a temperature that ran from 25°C to 750°C at a rate of 10°C min^{-1}, under air.

Results

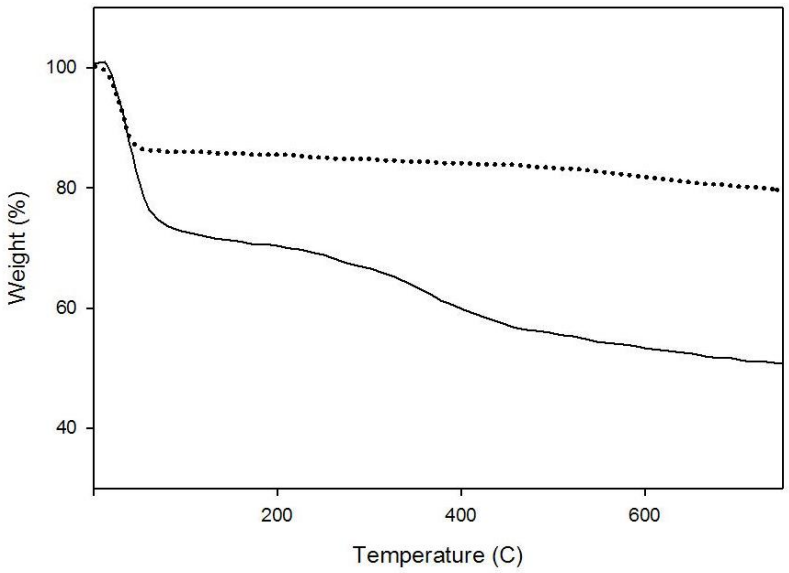

Figure 2.3 – TGA of $mSiO_2@Fe_2O_3$, 1) after furnace treatment (dotted line) or 2) washed with an ethanol/acetic acid mixture (solid line).

The furnace treated $mSiO_2@Fe_2O_3$ initially lost 13.3 % of its weight (25 to 57.5 °C) (*Figure 2.3*, *dotted line*) and there was no significant further weight loss. The $mSiO_2@Fe_2O_3$ cleaned of surfactant by refluxing for 2 hours in a solution containing ethanol, deionised water and glacial acetic acid, showed significantly greater weight loss on heating. This occurred in three stages (*Figure 2.3*, *solid line*). The first, from 25 to 57.5 °C with 28 % weight loss and the second, from 200 to 450 °C were due to volatilization of organic compounds and physically adsorbed water. The third weight loss, between 450–800°C of 5.5 %, may be due to condensation of the silanol groups to siloxane bonds with elimination of water [10].

2.6.4 Morphology and Size Distribution

Method

A Philips XL-30 scanning electron microscope was employed, which was equipped with an energy dispersive x-ray detector (EDX).

For high vacuum microscopy, the sample was prepared by sonicating *ca.* 5 mg of the substance for 1 hour in 50 mL of methanol and applying 1 small drop of the suspension onto a very clean, acetone washed glass slide (1 cm^2), which was fixed to an aluminium stud. To avoid electrical charging the samples were then coated with a *ca.* 10 nm thick gold film. A Hummer sputtering system (Anatech Ltd) was employed, using the conditions summarized in *Table 2.3*. The sample was then ready for SEM. The size of 100 particles was measured directly from the SEM picture to obtain the size distribution shown in *Figure 2.4b*.

Parameter	Value
Gas employed	Argon 5 psi
Current	~ 15 mA
Time of coating	1 minute

Table 2.3 – Sample preparation for the SEM.

Results

Figure 2.4a shows an SEM micrograph of the mSiO_2@Fe_2O_3 particles. These seem to have a spherical shape and, if sonicated long enough, they can be completely dispersed in solution. *Figure 2.4b* shows their size distribution, from 277 to 1011 nm. Most of the particles range from 523 to 769 nm.

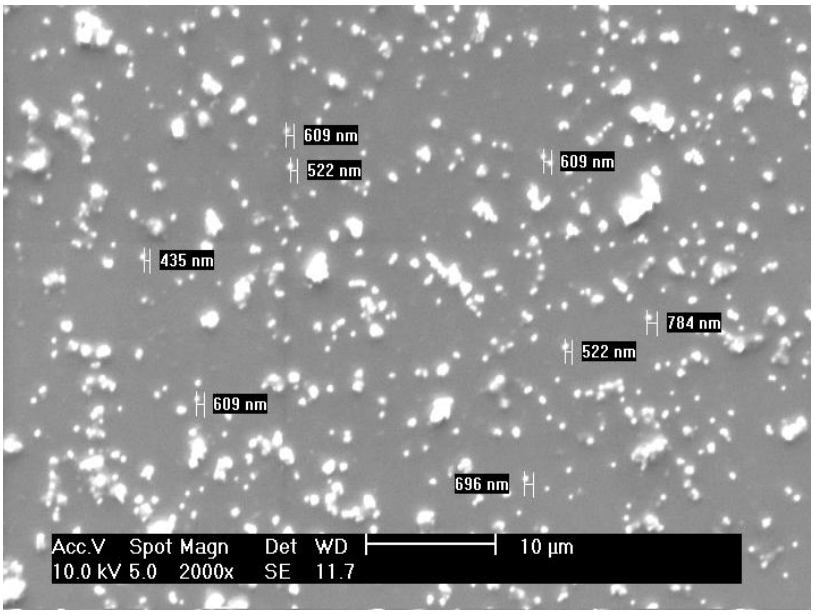

a)

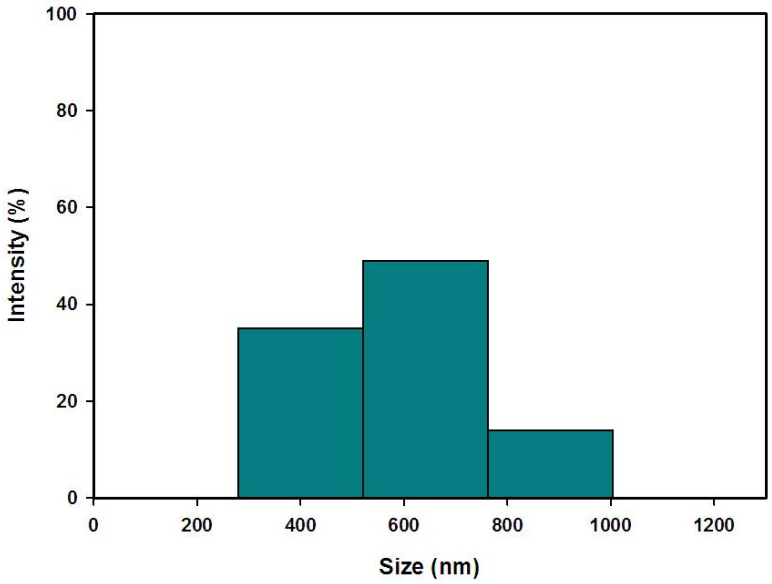

b)

Figure 2.4 – a) SEM picture of $mSiO_2@Fe_2O_3$, b) particle size distribution.

2.7 Characterization of Mesoporous Silica Particles

2.7.1 Fourier Transform Infrared Spectroscopy

Method

The method and instrument were as described in *Section 2.6.1*.

Results

The spectrum of the iron free silica (*Figure 2.5*), is very similar to the one shown in *Figure 2.1b* with the absence of the 567 cm^{-1} Fe-O stretching peak and a more prominent peak at 800 cm^{-1}.

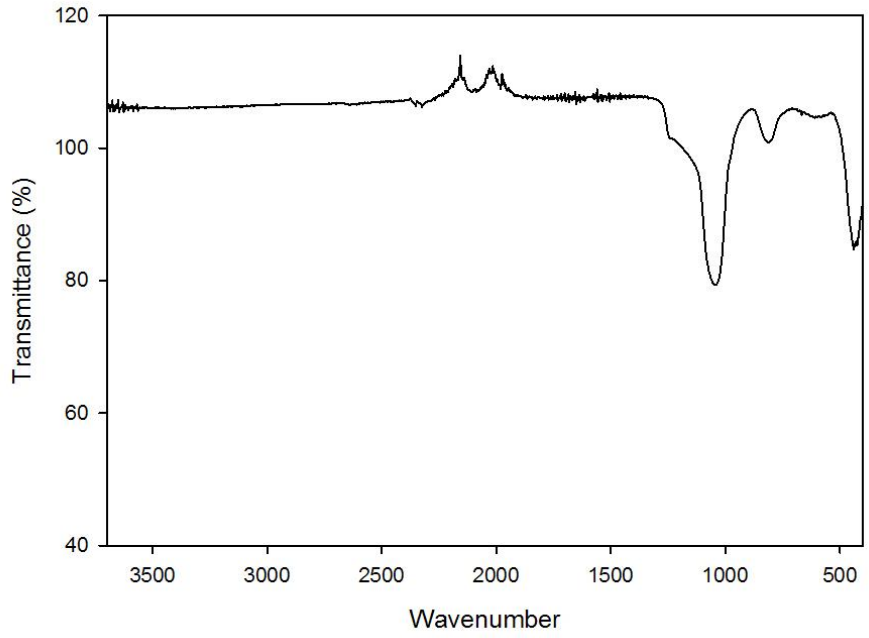

Figure 2.5 – FT-IR of $mSiO_2$ particles.

2.7.2 BET

Method

The instrument and technique were as described in *Section 2.6.2*.

Results

The adsorption-desorption isotherm of a $mSiO_2$ sample is shown in *Figure 2.6a*. The curves are very similar to those shown in *Figure 2.2a*. The formation of a hysteresis loop is still visible, even though the loop this time it is smaller. This narrow loop can indicate a narrow pore size distribution. *Figure 2.6b* the BET plot and *Table 2.4* shows the results obtained. Most notably the surface area of the $mSiO_2$ is approximately three times that of $mSiO_2@Fe_2O_3$. Both materials however have similar pore diameters in the mesoporous range.

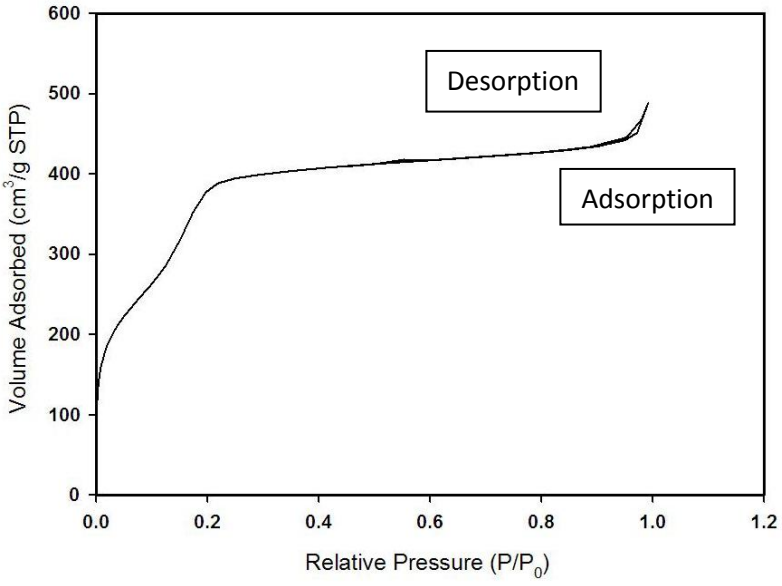

a)

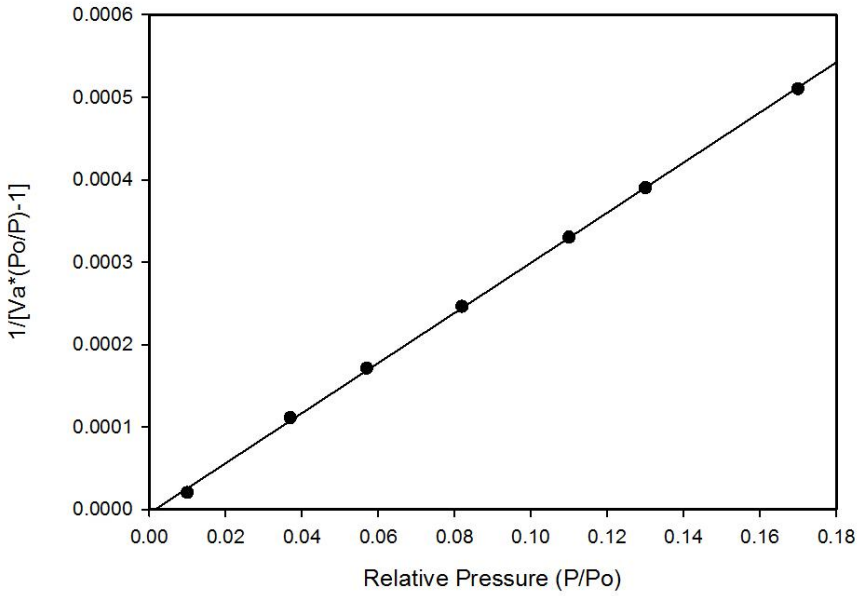

b)

Figure 2.6 – a) N_2 adsorption-desorption isotherms of $mSiO_2$. b) Corresponding BET plot.

BET multipoint surface area (m^2g^{-1})	1470
Total pore volume (cm^3g^{-1})	0.7358
Average pore diameter (Å)	134

Table 2.4 – BET results.

2.7.3 Thermogravimetric Analysis

Method

The instrument and technique were as described in *Section 2.6.3*.

Results

Thermal analysis of the $mSiO_2$ and $mSiO_2@Fe_2O_3$, (*Figure 2.7* and *Figure 2.3* (dotted line)) shows essentially identical behavior with a small initial weight loss due to physisorbed water. The sample had been treated in a furnace to remove the surfactant and no residual combustible material can be found in these samples.

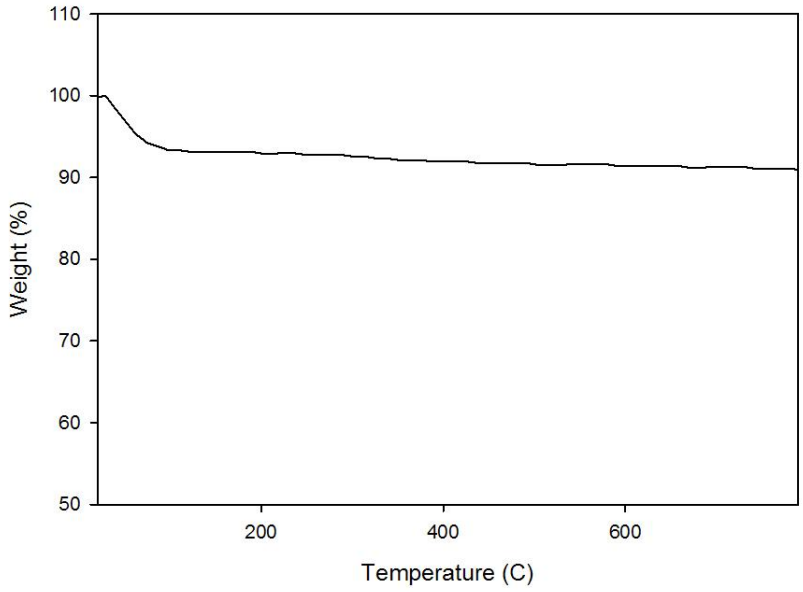

Figure 2.7 – TGA of the $mSiO_2$ particles.

2.7.4 Morphology and Size Distribution

Method

The instrument and technique were as described in *Section 2.6.4*.

Results

SEM of the $mSiO_2$ shows spherical particles (*Figure 2.8a*) with sizes from 171 to 346 nm *Figure 2.8b*. The most of the particles are within the 232 to 289 nm range. The $mSiO_2$ particles are therefore smaller than the $mSiO_2@Fe_2O_3$ and have a narrower size distribution.

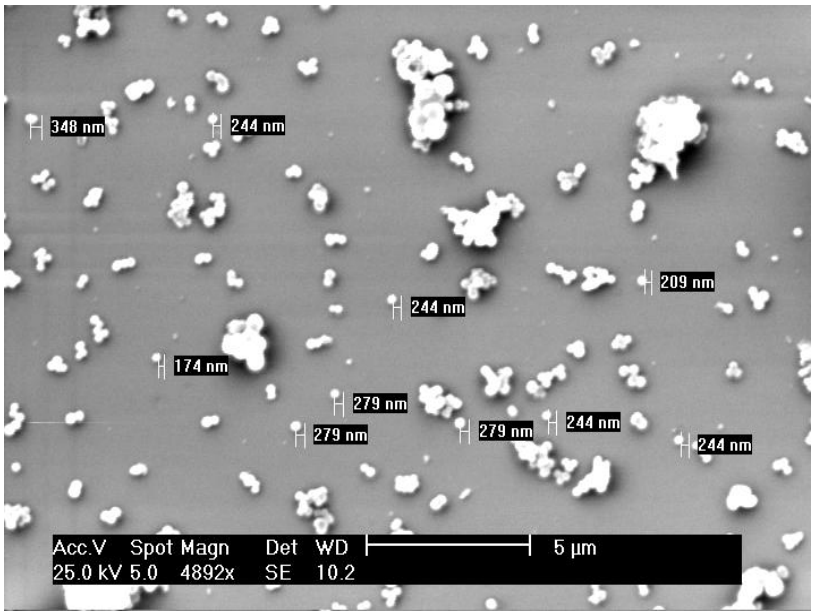

a)

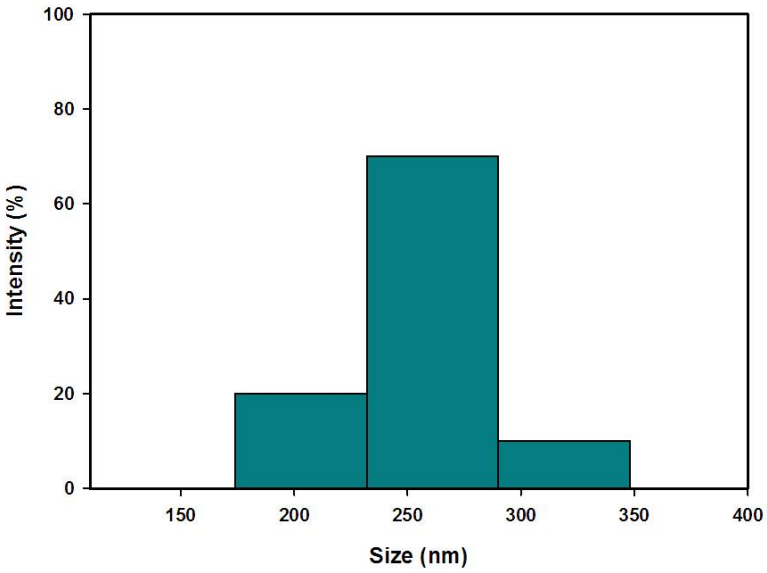

b)

Figure 2.8 – a) SEM picture of $mSiO_2$, b) size distribution.

2.8 Synthesis of $NH_2@mSiO_2@Fe_2O_3$ and $NH_2@mSiO_2$

$mSiO_2@Fe_2O_3$ and $mSiO_2$ particles were both modified with an organosilane giving them free amino groups exploitable for further chemical modification or direct application in metal ion extractions. In the next *Chapter* their conversion to dithiocarbamates will be described to enhance their chelating properties.

Method

1 g of $mSiO_2@Fe_2O_3$ or $mSiO_2$ was dispersed in 200 ml water (Solution A). 3 ml of 3-aminopropyltriethoxysilane (APTS) was dispersed in 150 ml water and the pH was adjusted to 4.3 with glacial acetic acid (Solution B). Solution B was then

added to solution A dropwise while stirring. This mixture was stirred vigorously for 2 hours at 70/80 °C. The particles were washed as described in *Method 1*.

2.9 Measurement of NH_2- Groups by Colourimetry

Ninhydrin is commonly used to detect ammonia or primary and secondary amines. When reacting with these free amines, a deep blue or purple colour known as Ruhemann's purple is developed (*Figure 2.9*) and this can be measured by visible spectrophotometry. Ninhydrin is most commonly used to detect peptides and proteins, but it can also be used to detect amino groups bound to a silica surface [11] [12].

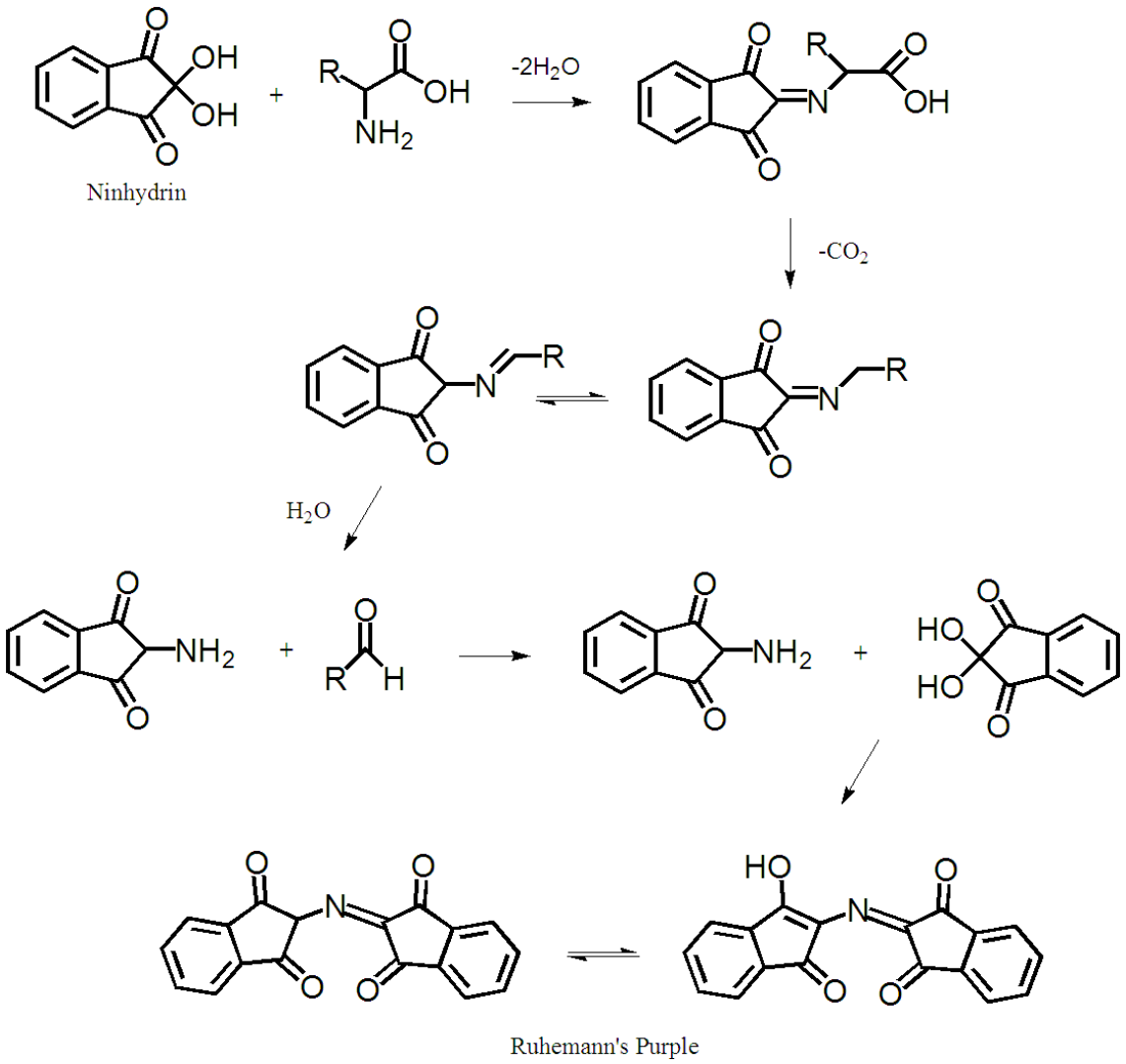

Figure 2.9 – Ruhemann's purple formation mechanism.

2.9.1 Ruhemann's Purple Deterioration

Ruhemann's purple once formed may undergo deterioration over time. A simple experiment was carried out in order to check if and how fast this occurs and therefore how long the samples could be stored before measurement.

Method

5 mL of a pH 6.5 buffer solution (phosphate 0.1 M) and 0.5 mL of ascorbic acid (1 g/L) were placed in a 20 mL glass vessel. 0.4 mL DL-valine (1 g/L) and 1 mL ninhydrin solution (5% w/w in ethanol) were added and the blue was developed keeping the samples in a water bath for 20 min at 80 °C solution. The blue solution was placed in a quartz UV-cuvette and this was placed in the spectrometer. The absorbance at 570 nm was monitored over a period of ca. 20 hours at room temperature.

Results

In *Figure 2.10* is plotted the absorbance vs. the elapsed time. The absorbance diminished by 40% over 20 hours and it is therefore not recommended to store the samples for any significant time once the blue colour has developed.

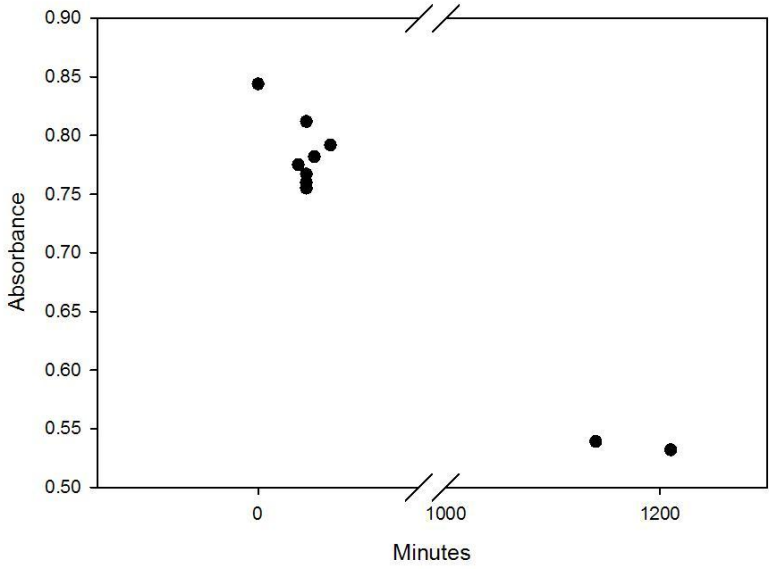

Figure 2.10 - Ruhemann's purple absorbance over the time.

2.9.2 Measurement

Method

The measurement of the amino groups on the modified surface of $mSiO_2@Fe_2O_3$ and $mSiO_2$ was carried out by a standard addition method, using the amino acid DL-valine as a calibrant. An accurately weighed mass (ca. 25 mg) of $NH_2@mSiO_2@Fe_2O_3$ was placed in three different 20 mL glass vessels. 5 mL of a pH 6.5 buffer solution (phosphate 0.1 M) and 0.5 mL of ascorbic acid (1 g/L) were added to each vessel. DL-valine (1 g/L) was added as calibrant in each vessel in different quantities (0, 0.2, 0.4 mL). 1 mL ninhydrin solution (5% w/w in ethanol) was then added to form the Ruhemann's Purple. The colour was developed by heating the mixtures in a water bath for 20 min at 80 °C. The particles were then attracted to a magnet and the blue solution was transferred into a 100 mL volumetric flask. 5 mL of water was then added to the remaining particles and the vessels were sonicated for a few seconds to help release residual coloured solution from the pores. The washings were added to the volumetric flask and the process was repeated until no further blue solution could be removed. All the volumetric flasks were made to 100 mL and the absorbance of each solution was measured at 570 nm in a quartz UV-cuvette using a Perkin-Elmer Lambda 3 UV-Vis spectrophotometer.

The same procedure was carried out for the $NH_2@mSiO_2$ particles, but once the blue had formed, the mixture was transferred to a centrifuge tube and centrifuged. The supernatant was collected in a 100 mL volumetric flask. Blanks

were prepared as described above in this S*ection* using particles that had not been modified.

Results

Ruhemann's purple exhibits two absorbance maxima: 400 and 570 nm (*Figure 2.11*). The latter was chosen for the amine measurement.

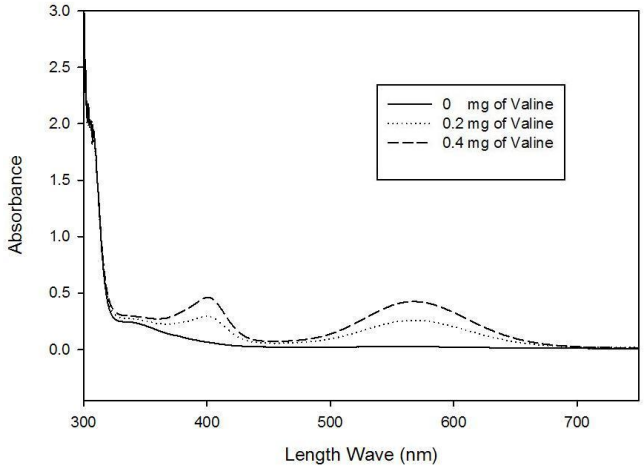

Figure 2.11 – Complete visible spectrum of Ruhemann's purple in water.

0.17 mmoles/g ± 5% of NH_2 were found on the surface of the $NH_2@mSiO_2@Fe_2O_3$ particles and 0.28 mmoles/g ± 5% on the $NH_2@mSiO_2$. Different surface areas of the two materials are probably the cause of this difference. Higher area means more space available for hosting the organosilane.

2.10 Conclusions

The synthesis and characterization of magnetic silica particles has been carried out by a variety of different synthetic methods. The highest silica content was obtained using a hexadecyltrimethylammonium chloride template to form mesoporous silica. Mesoporous silica particles (without a magnetic core) were also synthesized for comparison (*Chapter 3*).

N_2 isotherms from $mSiO_2@Fe_2O_3$ and $mSiO_2$ both had hysteresis loops and average pore diameters that lead to the conclusion that the silica is mesoporous. SEM pictures showed both type of particles to be spherical and have different sizes. Building a silica layer on the Fe_2O_3 resulted in $mSiO_2@Fe_2O_3$ particles that grew larger than $mSiO_2$.

FTIR spectra confirmed the presence of the silica layer and the absence of water, due to the furnace treatment during the synthesis. This fact can be seen in the TGA graphs, where the only weight loss is associated to the most weakly bound water, most likely originating from the atmosphere.

Functionalisation of the $mSiO_2@Fe_2O_3$ and $mSiO_2$ surfaces was carried out by reaction with 3-aminopropyltriethoxysilane and the extent of the modification was measured by means of the ninhydrin reaction. $mSiO_2@Fe_2O_3$ particles contained 0.17 mmoles/g and $mSiO_2$ 0.28 mmoles/g of amino groups. The difference is believed to be due to their different surface areas. The use of this organosilane material is described in *Chapter 3*, where the amino groups will be converted to dithiocarbamates and then employed in cation pre-concentration.

2.11 References

[1] C. Bethke, *Geochemical and biogeochemical reaction modeling*, 2nd ed., Oxford University Press, Cambridge, UK ; New York, **2008**.

[2] H.-H. Yang, S.-Q. Zhang, X.-L. Chen, Z.-X. Zhuang, J.-G. Xu, X.-R. Wang, *Analytical Chemistry* **2004**, *76*, 1316.

[3] D. K. Kim, Y. Zhang, J. Kehr, T. Klason, B. Bjelke, M. Muhammed, *Journal of Magnetism and Magnetic Materials* **2001**, *225*, 256.

[4] X. Liu, Z. Ma, J. Xing, H. Liu, *Journal of Magnetism and Magnetic Materials* **2004**, *270*, 1.

[5] P. Wu, J. Zhu, Z. Xu, *Vol. 14*, WILEY-VCH Verlag, **2004**, pp. 345.

[6] C. Graf, D. L. J. Vossen, A. Imhof, A. van Blaaderen, *Langmuir* **2003**, *19*, 6693.

[7] Y. Kobayashi, S. Saeki, M. Yoshida, D. Nagao, M. Konno, *Journal of Sol-Gel Science and Technology* **2008**, *45*, 35.

[8] S. Brunauer, H. Emmett, E. Teller, *Journal of the American Chemical Society* **1938**, *60*, 309.

[9] R. M. Cornell, U. Schwertmann, *The iron oxides: structure, properties, reactions, occurrences, and uses*, 2nd, completely rev. and extended ed., Wiley-VCH, Weinheim, **2003**.

[10] H. E. Bergna, W. O. Roberts, *Colloidal silica: fundamentals and applications*, CRC Taylor & Francis, Boca Raton, FL, **2006**.

[11] I. Taylor, A. G. Howard, *Analytica Chimica Acta* **1993**, *271*, 77.

[12] O. D. Shapilov, V. G. Kayumov, A. I. Krashenyuk, *Journal of Analytical Chemistry of the Ussr* **1983**, *38*, 436.

Chapter 3

Dithiocarbamated Particles

3.1 Introduction

Half-amide derivatives of dithiocarbonic acid, known as dithiocarbamates, are formed when a primary (eq. 3.1) or secondary (eq. 3.2) amine (in an alcoholic or aqueous solution) is reacted with CS_2 in the presence of an alkali metal hydroxide to form the corresponding salt:

$$RNH_2 + CS_2 + NaOH \rightarrow RNHCSSNa + H_2O \qquad (3.1)$$

$$R_1R_2NH + CS_2 + NaOH \rightarrow R_1R_2NHCSSNa + H_2O \qquad (3.2)$$

A very large number of literature works have been dedicated to dithiocarbamates as they have excellent metal ion binding properties [1]. Many applications have involved chelation of trace metals on a column of immobilized chelating agent; others have complexed the analytes in solution, followed by pre-concentration of the complex on a suitable substrate, such as C_{18} bonded silica or Amberlite XAD resins. Solvent extraction of dithiocarbamate complexes has been reported for the pre-concentration of a number of trace metal species from seawater [2]. The modification of silica surfaces using amino groups and subsequent conversion to mono- and bis-dithiocarbamates was introduced by Leyden et al. in 1976 [3]. Further investigation of silica functionalized with

dithiocarbamate was carried out by Taylor [4] and modified silica was used for the pre-concentration of trace metals from water. The authors mention that the bis-dithiocarbamate has twice the capacity of its diamine. The extraction of metal ions from ethanol was investigated by Espinola et al. [5]. They immobilized 3-propylethylenediamine on a silica surface, reacted it with carbon disulfide and obtained a dithiocarbamate group. Their product was employed to extract cobalt, nickel, copper and zinc ions. They found that the metal-ligand ratio depends on the type of cation. For instance, they found stoichiometric ratios of 1:3 for cobalt, 1:2 for nickel and 1:1 for copper and zinc. The anchoring of dithiocarbamate on silica gel has been investigated using solid state ^{29}Si MAS NMR, IR and sulphur analysis to confirm the conversion of the amino group to dithiocarbamate [6]. The dithiocarbamation of chitosan has been described [7], offering the possibility of binding it to magnetic nanoparticles, previously covered with chitosan.

Dithiocarbamates coordinate with transition metals in solution through the two sulphur atoms (*Figure 3.1*) [8], with more than one dithiocarbamate group normally being associated with each metal ion.

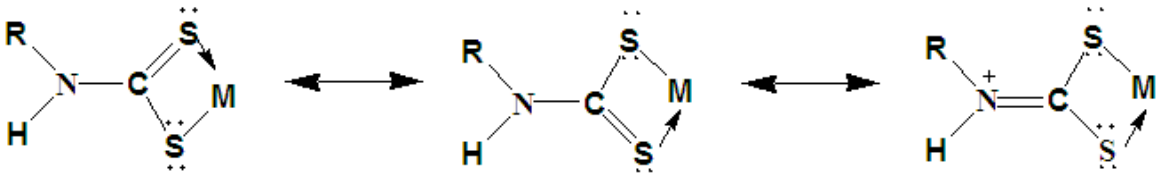

Figure 3.1 – DTC-metal complex.

The situation with dithiocarbamates attached to solid particles may differ from the solution case, in that the number of ligands attached to the metal may be subject to steric constraints. Absorption and release of copper in water under

both static and dynamic conditions may also be slower, due to the need for diffusion into the particles [9].

3.2 Materials

Aldrich (UK) supplied sodium hydroxide pellets, isopropanol and sodium acetate trihydrate (99%). Carbon disulfide was obtained from Rathburn. Copper sulphate pentahydrate (98%), borax (anhydrous, 98%) and iron (III) chloride hexahydrate (97%) were purchased by Sigma-Aldrich. 0.22 μm polymer membrane filters were obtained from Millipore.

3.3 Synthesis of DTC@mSiO$_2$@Fe$_2$O$_3$ and DTC@mSiO$_2$

This *Section* describes the synthetic methods adopted to convert NH$_2$@mSiO$_2$@Fe$_2$O$_3$ and NH$_2$@mSiO$_2$ to their dithiocarbamated derivatives.

Method

1 g of NH$_2$@mSiO$_2$@Fe$_2$O$_3$ or NH$_2$@mSiO$_2$ (synthesized as in *Section 2.8*) was placed in a 50 mL beaker containing 20 mL of aqueous 0.1 M sodium hydroxide solution, 5 mL isopropanol and 4 mL CS$_2$. The mixture was left stirring for 4 hours at room temperature. The DTC@mSiO$_2$@Fe$_2$O$_3$ particles were immobilized using a magnet, the supernatant was poured away, 30 mL of deionized water was added and the mixture was stirred for a few seconds. The supernatant was

removed and this operation was carried out 3 times with water and 3 times with isopropanol to remove unreacted chemicals. The particles were left to dry at room temperature. In case of the DTC@$mSiO_2$ the supernatant was separated by filtration using a syringe fitted with a 0.22 μm polymer membrane filter.

3.4 Evaluation of the Quantity of DTC Groups

Once DTC@$mSiO_2$@Fe_2O_3 and DTC@$mSiO_2$ have been synthesized, the effectiveness of the dithiocarbamation was evaluated.

Method

As described in *Section 2.9.2*, it is possible to measure the NH_2- groups by means of ninhydrin. The same procedure was carried out on DTC@$mSiO_2$@Fe_2O_3 and DTC@$mSiO_2$ particles (synthesised as described in *Section 3.3*). Knowing the amine content before and after the reaction with CS_2, it is possible to evaluate the degree of dithiocarbamation because for every 1 mol of DTC to have formed, 1 mol of NH_2- must have disappeared.

Results

Table 2.1 shows the amine content before and after reaction with CS_2. The amine content is significantly lower and their conversion to dithiocabamates was estimated as being ca. 90% for both the particle types.

Particles	Amine Content (mmol/g)	Amine Content (mmol/g)	Calculated DTC
DTC@mSiO$_2$@Fe$_2$O$_3$	0.17 ± 5%	0.022 ± 12%	87 %
DTC@mSiO$_2$	0.28 ± 5%	0.025 ± 9%	91 %

Table 3.1 – Yield of dithiocarbamation.

3.5 Effect of the Contact Time

The ion collecting properties of any modified silica depends, among other things, on the time allowed for the system to reach equilibrium. Ions require time to "migrate" from solution to the silica porous inner surface, where they can be collected by the functional groups. In this S*ection* the minimum time required was evaluated.

Method

Accurately weighed portions of DTC@mSiO$_2$ (25 mg) were placed in 8 glass vessels (25 mL each). 400 μL of a Cu^{2+} (1000 mg/L) solution and 20 mL of water were added to each vessel. Each vessel was mechanically shaken for a different length of time and then filtered by means of a syringe fitted with a 0.22 μm polymer membrane filter. The supernatant was transferred to a 50 mL volumetric flask and made up to volume with deionized water. The copper in solution was measured with a Perkin-Elmer 2380 atomic absorption spectrophotometer. Calibration was typically carried out over the range 1 to 10 μg/mL. Blanks were

prepared in the same way, but no Cu^{2+} ions were added. *Table 3.2* shows the parameters that were employed for the copper measurements.

Results

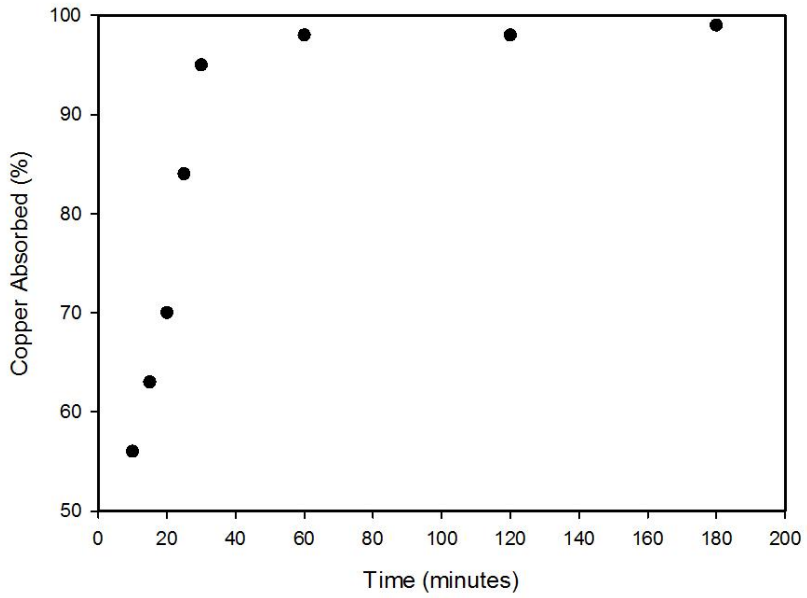

Figure 3.2 – Effect of contact time on copper absorption. 400 µg of Cu^{2+} recovered with 25 mg of DTC@mSiO₂

Measuring the copper left in solution allowed the copper collected by the DTC@mSiO₂ particles to be calculated as a function of contact time (*Figure 3.2*). The copper collected increased rapidly up to 30 minutes. No copper can be found in solution from this point onwards forward. In the subsequent experiments an equilibration period of 60 minutes was employed.

3.6 Copper Absorption Experiment

To be considered a good chelator for the purposes of trace metal pre-concentration, a chelating agent should show the following features in its pH/uptake curves:

- A broad flat plateau region centred on the sample pH that shows essentially 100% adsorption.
- A flat broad basal region with adsorption as near 0% as possible allowing full elution of the analyte from the chelator (usually very low pH).

The pH values chosen for this experiment (5, 7 and 9) cover the pH range of most natural waters. An experiment was carried out to evaluate the copper uptake onto all the particles used so far: Fe_2O_3, $mSiO_2@Fe_2O_3$, $NH_2@mSiO_2@Fe_2O_3$, $DTC@mSiO_2@Fe_2O_3$, $mSiO_2$, $NH_2@mSiO_2$, $DTC@mSiO_2$.

Method

500 mL of buffer solutions (0.1 M) were prepared at pH 5 (sodium acetate/acetic acid), pH 7 and pH 9 (borax/HCl) containing Cu^{2+} ions (5 mg/L). Each solution was also prepared without copper to be used for the blanks. Accurately weighed quantities (ca. 25 mg) of test material were placed in 25 mL glass vessels and 20 mL of buffer solution was added. For each pH three copper solution and three blank solutions were prepared. The samples were placed on a mixing wheel for 1 hour. The vessels containing magnetic particles were placed on a magnet and once the solution became clear the supernatant was poured into a 50 mL volumetric flask. The supernatant from the non magnetic materials was

separated by means of a syringe filter (0.22 μm polymer membrane) and placed in a 50 mL volumetric flask. All the volumetric flasks were made up to volume with deionized water.

The copper in solution was measured with a Perkin-Elmer 2380 atomic absorption spectrophotometer. Calibration was typically carried out over the range 1 to 10 μg mL^{-1}. *Table 3.2* shows the parameters that were employed for the copper measurements.

Element	Wavelength, nm	Slit Width, nm	Lamp, mA
Fe	248.2	0.7	7
Cu	324.8	0.7	5

Table 3.2 – Parameters for the AA measurement.

Results

Table 3.3 shows how the absorption of copper changed with pH and type of particles employed. All the particles absorbed copper because it can be trapped in the Fe_2O_3 lattice without any complex formation, but the absorption is not selective for a specific analyte and in a far more complex solution (for example, sea water) the particles collect some of almost everything. This "lattice effect" is largely reduced by the silica layer (see uptake for $mSiO_2@Fe_2O_3$) and in order to uptake metals efficiently and selectively, functional groups must be used. NH_2

and DTC groups bound Cu^{2+} strongly enough to absorb more than 90% of the copper (see uptake for $NH_2@mSiO_2$ and $DTC@mSiO_2$).

The most important thing to notice is the difference of behaviour between the particles with an iron-based magnetic core and the iron-free silica particles. As expected $NH_2@mSiO_2$ and $DTC@mSiO_2$ particles absorbed all the copper in solution at every pH and this is a sign of interaction between Cu^{2+} ions and both the ligands. $NH_2@mSiO_2@Fe_2O_3$ and $DTC@mSiO_2@Fe_2O_3$ unexpectedly behaved in the opposite way. The most reasonable explanation for this is that something blocked the formation of the copper complex. The possible presence of iron in solution and its competition with copper for the "active sites" could be the cause.

Cu	pH 5	pH 7	pH 9
Fe_2O_3	78 ± 10%	90 ± 9%	84 ± 15%
$mSiO_2@Fe_2O_3$	11 ± 7%	47 ± 11%	36 ± 9%
$NH_2@mSiO_2@Fe_2O_3$	20 ± 5%	60 ± 17%	46 ± 3%
$DTC@mSiO_2@Fe_2O_3$	24 ± 8%	66 ± 8%	75 ± 7%
$mSiO_2$	8 ± 13%	36 ± 10%	34 ± 6%
$NH_2@mSiO_2$	90 ± 11%	97 ± 9%	94 ± 6%
$DTC@mSiO_2$	95 ± 13%	96 ± 5%	99 ± 3%

Table 3.3 – Copper per cent absorbed.

Therefore the iron content was also measured in the same samples using the same instrument and parameters shown in *Table 3.2*.

Table 3.4 shows the quantity (mmoles) of iron released into solution. Only samples based on Fe_2O_3 show this release of iron. Even the silica layer could not

completely prevent leaching from the Fe_2O_3 lattice. Its quantity is not negligible, considering that every 25 mg of solid contains ca. 0.004 mmoles of DTC and it can significantly jeopardize the collection of trace heavy metals such: Cu^{2+}, Zn^{2+}, and Cd^{2+}.

Fe	pH 5	pH 7	pH 9
Fe_2O_3	0.0019	0.0033	0.0033
$SiO_2@Fe_2O_3$	0.0022	0.0020	0.0021
$NH_2@Fe_2O_3$	0.0015	0.0074	0.0069
$DTC@Fe_2O_3$	0.0015	0.0016	0.0016
$mSiO_2$	0	0	0
$NH_2@mSiO_2$	0	0	0
$DTC@mSiO_2$	0	0	0

Table 3.4 – mmoles of iron measured in solution.

3.7 Behaviour of $DTC@mSiO_2$ in the Presence of Fe^{3+}

An experiment was carried out to confirm that the formation of the DTC-Cu^{2+} complex is obstructed by the presence of Fe^{3+}.

Method

Accurately weighed quantities (ca. 25 mg) of $DTC@mSiO_2$ were placed in 6 glass vessels (25 mL) and 20 mL of pH 7 buffer solution (Borax/HCl) was added to each. 200 µL of a 1000 mg/L Cu^{2+} solution and different volumes of a 1000 mg/L

Fe^{3+} solution were added to each vessel. The samples were mixed by means of a stirring wheel for 1 hour. The supernatants were separated by means of a syringe fitter (0.22 μm polymer membrane filter) and placed in 50 mL volumetric flasks. All the volumetric flasks were made up to volume with deionized water and the copper and iron contents of these solutions were analysed by atomic absorption spectroscopy, as described in *Section 3.6.1*.

Results

Figure 3.3 shows the collection of copper as the Fe^{3+} concentration is increased. At low iron concentration both copper and iron are completely taken up by the particles; there are sufficient "active sites" to accommodate every metal ion in solution. Increasing the iron content however, prevented copper from complexing on the particles. The artificial addition of iron has therefore confirmed that DTC functional group cannot be used in extraction of copper when the environment contains significant quantities of iron. Sufficient iron is released from the magnetic DTC silica particles to cause difficulties with its application.

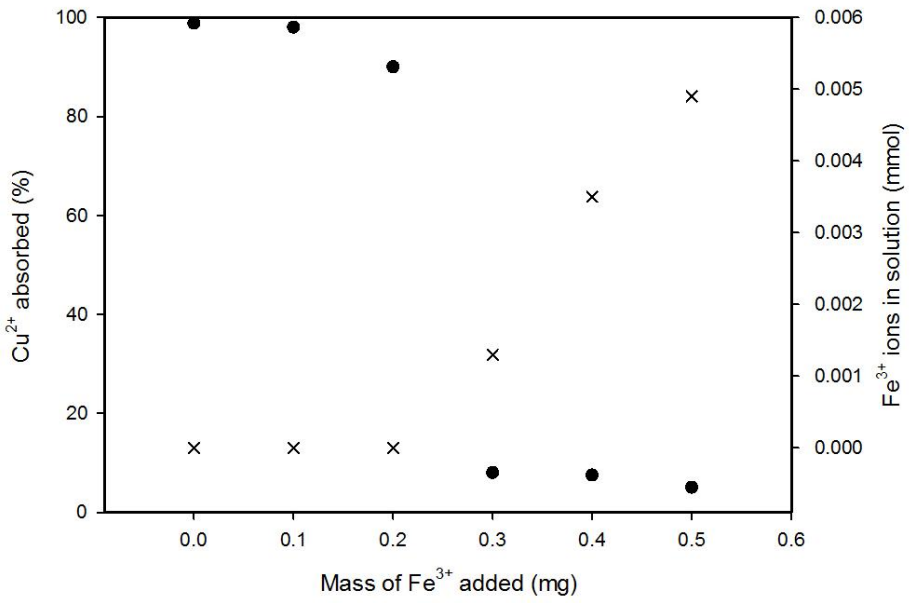

Figure 3.3 – Cu^{2+} absorption in presence of Fe^{3+}.

3.8 Conclusions

Dithiocarbamated magnetic silica particles were successfully synthesized and their dithiocarbamate groups were estimated by the measurement of residual amine groups left after $NH_2@mSiO_2@Fe_2O_3$ and $NH_2@mSiO_2$ had reacted with CS_2. Conversion to DTC was found to have been around 87% and 91% respectively.

The effect of contact time on copper absorption was studied and 1 hour was found to be sufficient for complete metal ion scavenging from solution, allowing the ions to reach the inner active sites of the silica.

Copper absorption experiments at different pH values were carried out. The copper-uptake performances of materials containing Fe_2O_3 were inferior to pure silica-based materials under identical experimental conditions. Iron that had

leached from the Fe_2O_3 lattice was found in solution and this can compete against copper ions for the DTC groups.

At this point of the project pre-concentration of trace heavy metals by means of DTC@mSiO_2@Fe_2O_3 was considered not to be promising and an alternative system was therefore studied.

3.9 References

[1] R. A. Nickson, S. J. Hill, P. J. Worsfold, *Analytical Proceedings* **1995**, *32*, 387.

[2] J. D. Lee, J. M. Lo, *Analytica Chimica Acta* **1994**, *287*, 259.

[3] D. E. Leyden, G. Howard Luttrell, A. E. Sloan, N. J. DeAngelis, *Analytica Chimica Acta* **1976**, *84*, 97.

[4] I. Taylor, PhD thesis, University of Southampton (Southampton), **1991**.

[5] J. G. P. Espinola, J. M. P. Defreitas, S. F. Deoliveira, C. Airoldi, *Colloids and Surfaces a-Physicochemical and Engineering Aspects* **1994**, *87*, 33.

[6] K. A. Venkatesan, T. G. Srinivasan, P. R. Vasudeva Rao, *Colloids and Surfaces A: Physicochemical and Engineering Aspects* **2001**, *180*, 277.

[7] E. Humeres, E. P. de Souza, N. A. Debacher, A. E. Aliev, *Journal of Physical Organic Chemistry* **2002**, *15*, 852.

[8] A. Ariafard, M. M. Amini, R. Fazaeli, H. R. Aghabozorg, *Journal of Molecular Structure-Theochem* **2004**, *672*, 141.

[9] B. Perez-Cid, S. Rio-Segade, C. Bendicho, *Microchemical Journal* **1997**, *55*, 319.

Chapter 4

C_{18} Modified Particles

4.1 Introduction

Octadecylsilane-modified silica was principally introduced to analytical chemistry as a packing material for HPLC columns. The materials were prepared by coupling an n-octadecylsiloxane to the surface of a support [1]. One of the most useful applications of these materials is the separation of organic pollutants from water prior to their measurement by chromatographic techniques. Herbicides, polynuclear aromatic hydrocarbons, chlorinated pesticides and phthalates have all been successfully extracted by solid-phase extraction with octadecyl-modified silicas [2] [3] [4] [5] [6].

The aim of the research reported in this chapter was to assess the possibility of anchoring octadecyltrichlorosilane groups on the surface of $mSiO_2@Fe_2O_3$ particles and to test this new material for the pre-concentration of polynuclear aromatic hydrocarbons (PAH) and tributyltin (TBT) compounds.

4.2 Materials

Octadecyltrichlorosilane (90%) was obtained from Aldrich (UK). A stock solution of polynuclear aromatic hydrocarbons was purchased from Supelco (100-2000

μg/ml of each compound in CH_3OH:CH_2Cl_2(1:1)). 1-hexadecanol (99%), octadecane (98%), octadecanol (98%) and glycol triethylene dimethylether (99%) were obtained from Aldrich (UK). Potassium hydroxide and hexane were purchased from Fisher Scientific (UK).

4.3 Synthesis of C_{18}@mSiO_2@Fe_2O_3

Octadecyltrichlorosilane is highly active and reacts with silica-based silanol groups at room temperature, with no need for a base catalyst. In the first step (*Figure 4.1a*), the silane molecule is hydrolyzed by available water in the silica surface, eliminating HCl. The hydroxyl group on the silica surface reacts with the silanol that has been formed and eliminates water forming a covalent bond with the surface [7] (*Figure 4.1b*). The remaining hydroxyl groups on the octadecylsilane can react with other surface silanols or with the silanols on neighbouring silane molecules, thereby forming a cross-linked polymer layer. However, a silane molecule can form only two bonds with the surface, due to steric hindrance, and a third bond with a neighbouring silane molecule [8].

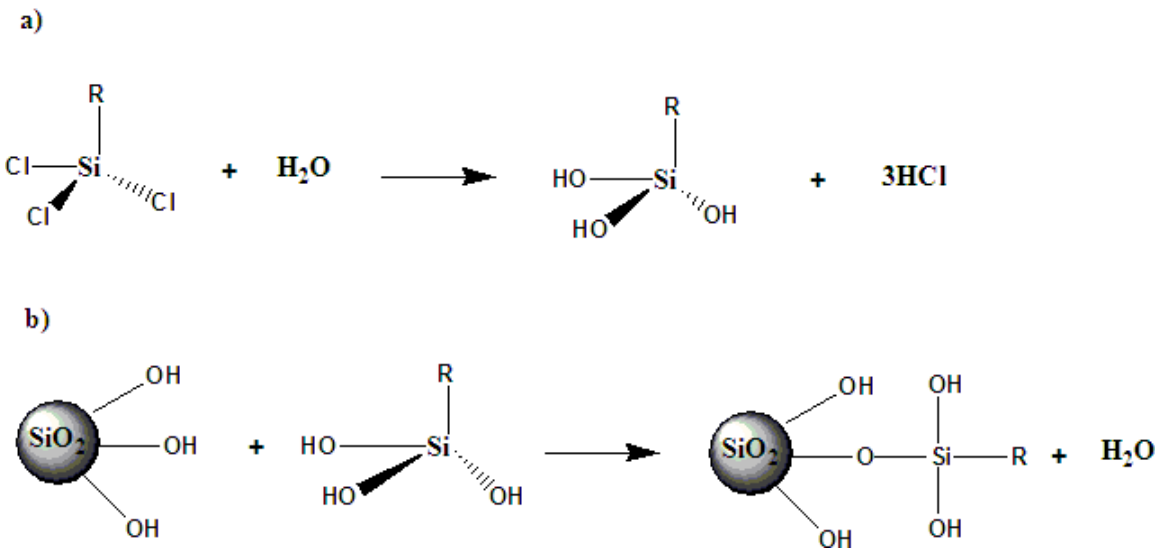

Figure 4.1 – a) Hydrolysis of the silane molecule and b) reaction with the silica surface.

The effect of different parameters, such as temperature and water concentrations, can have big influence on the final product. A trace of water is essential to the silanation reaction and a low temperature is favourable for immobilisation.

Method

2 g of $mSiO_2@Fe_2O_3$ was dispersed in 50 ml dry toluene and sonicated for 1h. The toluene was poured out of the vessel, retaining the particles with an external magnet. 200 ml of fresh dry toluene was added and under stirring, 0.5 ml of octadecyltrichlorosilane was added dropwise. The solution was left stirring for 2 hours at room temperature. The particles were immobilized using a magnet, the supernatant was poured away, 20 mL of toluene was added to the solid and the mixture was stirred for a few seconds. The supernatant was removed and this

operation was carried out 3 times to remove unreacted chemicals. The particles were left to dry at room temperature.

4.4 Characterization

Once the C_{18}@mSiO_2@Fe_2O_3 particles had been synthesised, characterization was carried out.

4.4.1 Fourier Transform Infrared Spectroscopy

Method

The instrument and technique were as described in *Section 2.6.1.*

Results

Figure 4.2 shows the FTIR spectrum of the C_{18}@mSiO_2@Fe_2O_3 particles. Peaks at 1060, 800 and 440 cm^{-1} were attributed to the Si-O stretching vibrations and the peak at 567 cm^{-1} was due to the stretching of the Fe-O bond. The same peaks were present in the spectrum of the mSiO_2@Fe_2O_3 particles (*Figure 2.1b*). Peaks at 2866 and 2770 cm^{-1} show the presence of C-H stretching vibration and the possibility of the C_{18} chain on the surface. These peaks may be considered quite large, considering the quantity of C_{18} involved and the presence of residual solvent may have affected their formation. Therefore this spectrum cannot be considered as a definite proof of the presence of a modified surface.

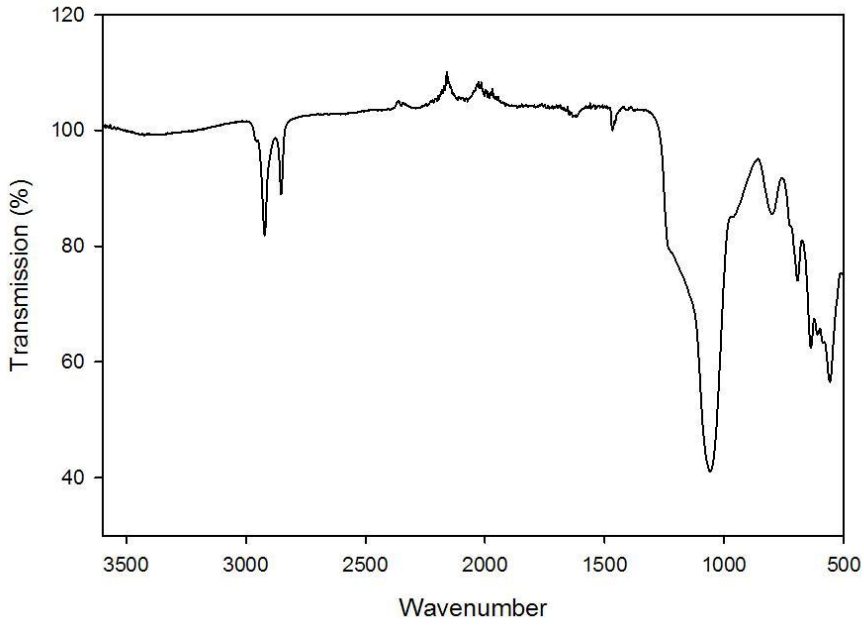

Figure 4.2 – FTIR spectrum of C_{18}@SiO_2@Fe_2O_3.

4.4.2 Thermogravimetric Analysis

Method

The instrument and technique were as described in *Section 2.6.3.*

Results

Figure 4.3 shows the TGA graph of C_{18}@mSiO_2@Fe_2O_3. 2% weight loss until 220 °C was observed, probably caused by evaporation of residual solvent and water (from atmospheric adsorption).

The main weight loss (15%) was observed between 220 and 700°C due to the decomposition of octadecyl groups and changes in the silica [9]. A 15% loss corresponds to 149 mg of C_{18} per 1 g of $C_{18}@mSiO_2@Fe_2O_3$. 246 mg of octadecyltrichlorosilane (d=0.984 g/ml) was available in the reaction for 1 g of particles and 60% of is thought to be bound to the surface. It is not possible to tell how often crosslinking occurred among the chains.

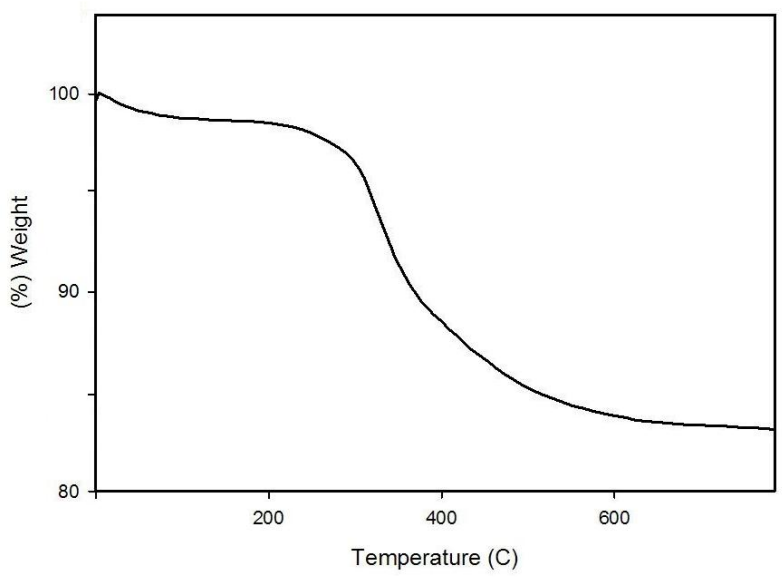

Figure 4.3 – TGA of $C_{18}@mSiO_2@Fe_2O_3$.

4.4.3 Morphology and Size Distribution

Method

The instrument and technique were as described in *Section 2.6.4.*

Results

Figure 4.4a shows an SEM micrograph of the C_{18}@mSiO_2@Fe_2O_3 particles. The reaction with the C_{18} chain did not change their spherical shape and the particles could be completely dispersed in a methanol solution. *Figure 4.4b* shows their size distribution.

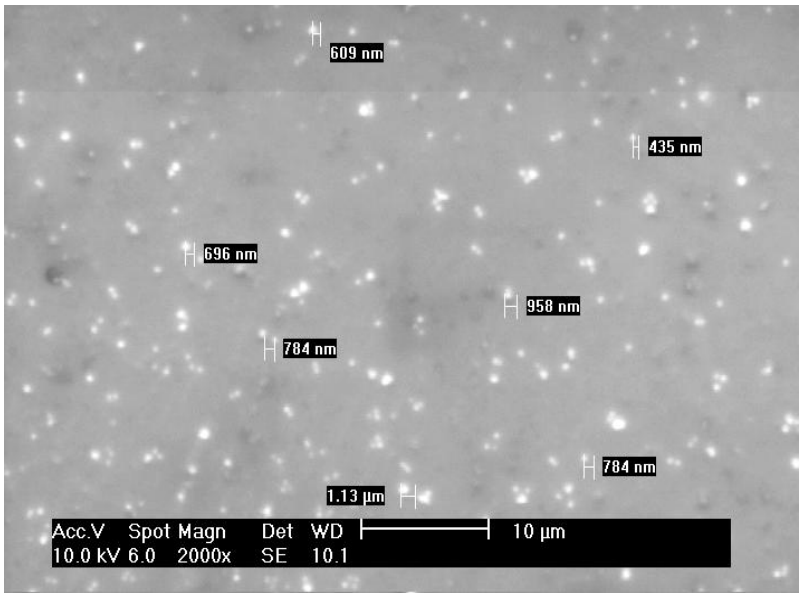

a)

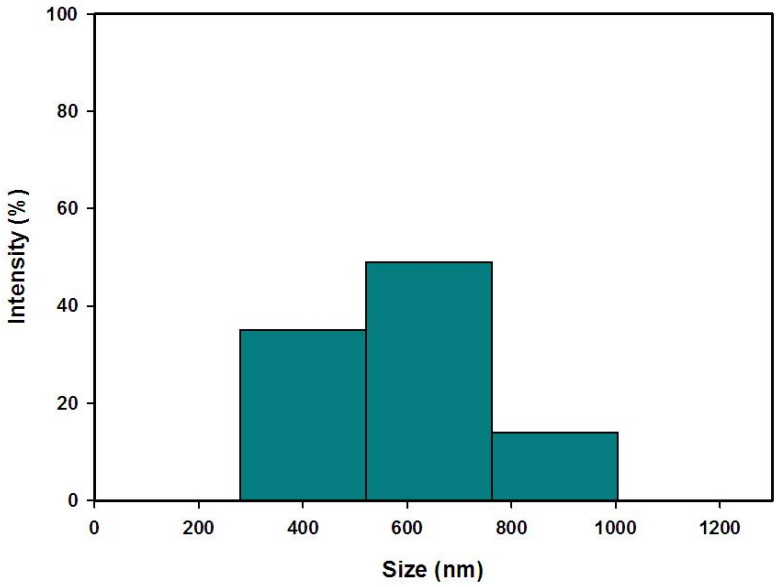

b)

Figure 4.4 – a) SEM micrograph of C_{18}@$mSiO_2$@Fe_2O_3 and b) particle size distribution.

4.4.4 Quantitative Assessment of the C_{18} Loading

The loading of octadecyl groups on the silica surface was assessed using a modification of the method described by Genieser et al. [10]. This is based on the release of both octadecane and octadecanol from the silica by fusion in potassium hydroxide. The estimate of octadecyl loading is obtained from the sum of the two products. The measurement was obtained by gas-chromatography.

Method

Calibration Curve

Stock solutions were prepared by dissolving 10 mg of octadecane, 1-octadecanol and hexadecanol in 10 mL of n-hexane. Appropriate dilutions were carried out to obtain mixtures containing octadecane, 1-octadecanol and hexadecanol (35, 200 and 50 μg mL^{-1}), (17.5, 100 and 50 μg mL^{-1}) and (8.75, 50 and 50 μg mL^{-1}), respectively. The concentration of hexadecanol was kept constant and used as an internal standard and the calibration curves for the measurement of octadecane and 1-octadecanol were constructed by dividing the heights of the analyte peaks by the height of the internal standard peak. The chromatography was carried out using a Perkin-Elmer 8500 Chromatograph fitted with flame ionization detection (FID) and a SA-1 fused silica quartz capillary column. Splitless injection was employed with a N_2 carrier gas flow rate of *ca.* 1 mL min^{-1}. The temperature program and retention times are reported in *Table 4.1*.

Temperatures Program	Settings
Step 1	3 min. at 60 °C
Step 2	Rise to 160 °C (20 °C/min.)
Step 3	Rise to 200 °C (3 °C/min.)
Step 4	Rise to 250 °C (30 °C/min.)
Step 5	15 min. at 250 °C
Injector Temperature	300 °C
Detector Temperature	300 °C

a)

Compounds	Retention Time (min.)
Octadecane	22.62
Hexadecanol	24.61
Octadecanol	28.05

b)

Table 4.1 a) – GC temperature program and b) retention times.

Sample Preparation

C_{18}@mSiO_2@Fe_2O_3 particles were accurately weighed (50 mg) and transferred to a small test tube (x3). 100 mg of KOH was added to each tube and the mixture was left overnight in a desiccator containing P_2O_5. 200 µl of triethylene glycol dimethylether was added to each tube. The tubes were placed in a metal heating block on a hot plate and heated at 216 °C for 2 hours. After cooling to room temperature, 250 µl of H_2O were added to each tube, followed by 100 µl of a hexadecanol solution (1 mg/ml of hexadecanol in hexane) as internal standard. 140 µl of HCl (37% (w/v)) was added to each tube. The tubes were shaken for 10 seconds and 500 µl of n-hexane was finally added to each. The mixture was shaken for 1 minute. The tubes were centrifuged and the hexane layer was transferred to a 2 ml volumetric flask and made up to volume with n-hexane. The sample was then measured by GC, using the same conditions and instrument used to construct the calibration curve. The peak heights of the released analytes were divided by the height of the internal standard peak to derive their concentrations from the calibration curve.

Results

Table 4.2 reports the mass of octadecyltrichlorosilane per gram of particles. Comparing this result with the TGA graph shown in *Figure 4.4.2*, the amount of organic material appears significantly lower. The synthetic conditions (especially temperature and trace water) can affect how the C_{18} chains are placed on the surface [7]. The optimal situation occurs when they make a monolayer and the octadecyltrichlorosilane can be decomposed quantitatively to octadecane and octadecanol. Probably this is not what happened during the experiment and the measurement gave a lower mass. The C_{18} chains should maintain their sorbent properties.

Compounds	C_{18} loading mg/g
Octadecane	**0.2 ± 7%**
Octadecanol	**1.5 ± 11%**
Octadecane + Octadecanol	**1.7 ± 10%**

Table 4.2 – Mass of C_{18} chain per gram of particles.

4.4.5 Hydrophobicity

C_{18}@mSiO_2@Fe_2O_3 cannot be dispersed directly in water due to the hydrophobicity of the C_{18} chains. In order to use these particles in a water sample, it is necessary to disperse them in a suitable solvent before use. This solvent must be miscible with water and leave the particles well separated after sonication. Typically the particles were sonicated for a few minutes in 20 ml of methanol before adding them to a water sample.

4.5 Extraction and Measurement of PAHs

This *Section* reports preliminary experiments in which C_{18}@mSiO_2@Fe_2O_3 particles are used to pre-concentrate PAHs from water. The experiments can be divided into four parts: absorption of 16 PAHs (Supelco, *Section 4.2)* onto the particle surface, their extraction from the particles by means of a suitable solvent, reduction of the final volume before the measurement (blow down phase) and their final measurement by gas chromatography. During the blow down it is very common to lose analytes, especially the ones with higher volatility. This loss was assessed for each PAH before the pre-concentration experiment was carried out.

4.5.1 Blow Down

Method

A commercial PAH standard solution from Supelco was divided in two parts and diluted with two different solvents having different miscibilities and used in different parts of the experiment. 500 µl of the standard solution was transferred to a 5 ml volumetric flask and made up to volume with methanol (Solution A). Another 500 µl was transferred to new 5 ml volumetric flask and made up to volume with n-hexane (Solution B). 100 µl of Solution B was added to a beaker containing 20 ml of dichloromethane and the beaker was placed on a metal hot plate to aid the vaporisation of the solvent. Periodically fresh dichloromethane was added with a pipette to clean the walls of the beaker of residual PAHs and to gather them in the bottom of the beaker. Before it was completely dry, the solution was transferred to a smaller vessel. Once dry, 1 ml of n-hexane was

added. 1 µl of this solution was ready to be measured. 100 µl of Solution B was diluted to 1 ml and analyzed by gas chromatography as a control. This experiment was repeated 5 times.

Gas Chromatography

A Perkin-Elmer 8500 Gas Chromatograph with flame ionization detection was used for the polynuclear aromatic hydrocarbons analysis. The instrument was fitted with a SA-1 fused silica quartz capillary column. 1 µl was injected into a splitless injector. The temperature program is reported in *Table 4.3*.

Temperatures Program	Settings
Step 1	3 min. at 50 °C
Step 2	Rise to 190 °C (20 °C/min.)
Step 3	10 min. at 190 °C
Step 4	Rise to 300 °C (10 °C/min.)
Step 5	60 min. at 300 °C
Injector Temperature	300 °C
Detector Temperature	300 °C

Table 4.3 – GC Temperature program.

Results

Recoveries were calculated based on the ratio of compound peak height with and without blow down (*Table 4.4*). These values are going to be added up to values obtained in the next pre-concentration experiment, in order to assess the real capacity of the particles.

PAH	Recovery	Loss
Napthalene	0 ± 10%	100 ± 10%
Acenaphthylene	33 ± 11%	67 ± 11%
Acenaphthene	40 ± 3%	60 ± 3%
Fluorene	37 ± 11%	63 ± 1%
Phenanthrene	70 ± 3%	30 ± 3%
Anthracene	71 ± 6%	29 ± 6%
Fluoranthene	53 ± 7%	46 ± 7%
Pyrene	89 ± 11%	11 ± 11%
Benz(a)anthracene	90 ± 6%	10 ± 6%
Chrysene	97 ± 4%	3 ± 4%
Ben(b)fluoranthene	82 ± 3%	18 ± 3%
Benz(k)fluoroanthene	80 ± 3%	20 ± 3%
Benzo(a)pyrene	91 ± 4%	9 ± 4%
Indeno (1,2,3-cd)pyrene	82 ± 3%	18 ± 3%
Dibenzo(a,h)anthracene	85 ± 6%	15 ± 6%
Benz(ghi)perylene	81 ± 7%	19 ± 7%

Table 4.4 – Recoveries of PAH after solvent evaporation.

The most volatile PAHs are greatly affected by the evaporation process, experiencing more than 60% loss.

4.5.2 Pre-concentration from Water Samples

Both the C_{18}@mSiO_2@Fe_2O_3 and its parent mSiO_2@Fe_2O_3 were assessed for their abilities to take PAHs from aqueous solution.

Method

100 µl of Solution A (*Section 4.5.1*) was transferred into a 100 ml volumetric flask and 50 ml of deionised water was added. 200 mg of C_{18}@mSiO_2@Fe_2O_3 or mSiO_2@Fe_2O_3 particles was placed in a beaker containing 5 ml of methanol and sonicated for 15 minutes. The dispersed particles were then added into the volumetric flask and the volume was made up to the mark with deionised water. The flask was mechanically mixed for 1 hour. The content of each flask was transferred into a beaker and a magnet was used to immobilize the particles and the supernatant was poured away. 20 ml of dichloromethane was added to extract the PAHs from the solid and this was collected in another smaller beaker. The blow down process and measurement were then carried out as described in *Section 4.5.1*. The experiment was repeated 3 times. The same experiment was also carried out recovering 100 µl of Solution A from 1000 ml of water.

Results

PAH	Recovery From 100 ml
Napthalene	0 ± 12%
Acenaphthylene	1 ± 8%
Acenaphthene	0 ± 5%
Fluorene	0 ± 15%
Phenanthrene	1 ± 20%
Anthracene	0 ± 10%
Fluoranthene	1 ± 7%
Pyrene	0 ± 12%
Benz(a)anthracene	1 ± 18%
Chrysene	0 ± 5%
Ben(b)fluoranthene	0 ± 7%
Benz(k)fluoroanthene	0 ± 11%
Benzo(a)pyrene	1 ± 4%
Indeno (1,2,3-cd)pyrene	0 ± 8%
Dibenzo(a,h)anthracene	1 ± 9%
Benz(ghi)perylene	0 ± 20%

Table 4.5 – Recovery of PAH from water using $mSiO_2@Fe_2O_3$.

PAH	Recovery From 100 ml	Recovery From 1000 ml
Napthalene	0 ± 3%	0 ± 7%
Acenaphthylene	80 ± 10%	81 ± 5%
Acenaphthene	77 ± 6%	85 ± 8%
Fluorene	82 ± 13%	78 ± 7%
Phenanthrene	90 ± 5%	87 ± 22%
Anthracene	79 ± 20%	75 ± 3%
Fluoranthene	84 ± 17%	90 ± 12%
Pyrene	82 ± 7%	83 ± 7%
Benz(a)anthracene	88 ± 14%	74 ± 12%
Chrysene	100 ± 6%	84 ± 22%
Ben(b)fluoranthene	98 ± 21%	93 ± 17%
Benz(k)fluoroanthene	69 ± 30%	74 ± 5%
Benzo(a)pyrene	87 ± 4%	80 ± 8%
Indeno (1,2,3-cd)pyrene	86 ± 9%	82 ± 13%
Dibenzo(a,h)anthracene	83 ± 12%	70 ± 13%
Benz(ghi)perylene	74 ± 10%	81 ± 9%

Table 4.6 - Recovery of PAH from water using $C_{18}@mSiO_2@Fe_2O_3$.

Tables 4.5 and *4.6* show the PAH recoveries from water using $mSiO_2@Fe_2O_3$ and $C_{18}@mSiO_2@Fe_2O_3$ particles respectively. In both cases the values are corrected for blow down.

In the first case the particles were not able to "trap" the analytes because they have no affinity with them. The high affinity of PAHs for the C_{18} chain is evident from the high recoveries to be found in *Table 4.5*. Recoveries of ca. 80% from both 100 and 1000 ml sample solutions are very promising considering that just masses from 1 to 20 μg of PAHs were spiked during the experiment. In a real water sample PAHs are generally present in ng per litre and the particles could be employed for their quantitative extraction. Similar methods have been extensively studied in literature using different solvents, C_{18} silica columns (or cartridges) and analytical techniques [11-15]. Generally, 80-90% of recovery from a solution with a concentration of a few ng per litre of PAHs is achieved. The PAHs employed in this project are considered the most dangerous for humans and therefore their detection is widely studied in literature. This new SFE method should be tested for environmental water samples using PAHs in lower quantities, in order to compare properly its performance with results found in other works.

4.6 TBT Extraction

This *Section* describes a pilot experiment to evaluate the extraction of TBT from water using the $C_{18}@mSiO_2@Fe_2O_3$ particles. The measurement procedure adopted was set up with the help of my colleague Awad Al-Rashdi, who worked

in our group. He had previously successfully recovered TBT from water using mesoporous silica particles having no magnetic core (C_{18}@mSiO_2).

Method

200 mg of C_{18}@mSiO_2@Fe_2O_3 was sonicated in 20 ml of ethanol. The suspension was transferred to a 100 ml volumetric flask and made up to the mark with deionised water. 5 µl of a 1 µg/ml (as TBT) solution was added to the flask using a Hamilton microliter syringe. The flask was left for 1 hour and periodically shaken, to assist the sorption. The solution was poured into a 250 ml beaker, the solid was attracted to the bottom with a magnet and the liquid was poured away. The solid was dried overnight in a vacuum desiccator using an activated silica gel desiccant.

1 ml of n-hexane and 1 ml of n-hexylmagnesium bromide Grignard reagent (2M in diethyl ether) were added to the beaker containing the dried particles. The reaction was left for 2 hours and 2 ml of HCl solution (5%) was then added to quench the excess Grignard reagent.

After the reaction had taken place, the aqueous layer was discarded and the hexane layer was dried with activated anhydrous sodium sulphate. The hexane layer was transferred to a 5 ml volumetric flask and the flask was made up to the mark with hexane. 1 µl was finally injected into a gas chromatograph which was fitted with a capillary column, coupled to a pulsed flame photometric detector. The temperature program is shown in *Table 4.7*.

Temperatures Program	Settings
Step 1	1 min. at 50 °C
Step 2	Rise to 100 °C (50 °C/min.)
Step 3	Rise to 130 °C (7 °C/min.)
Step 4	Rise to 270 °C (20 °C/min.)
Step 5	15 min. at 270 °C
Injector Temperature	150 °C, rise to 250 °C (40 °C/min.)

Table 4.7 – Temperature program.

Results

92±15 % recovery was achieved from a 50 ng/L spiked sample solution. This pilot experiment shows that the C_{18}@mSiO_2@Fe_2O_3 particles are able to extract TBT from water solution at a trace level. Even though this result was promising, because of lack of time, no further experiments were carried out.

4.7 Conclusions

C_{18}@mSiO_2@Fe_2O_3 particles have been successfully synthesised by reacting mSiO_2@Fe_2O_3 particles with octadecyltrichlorosilane. The presence of a C_{18} chain was proven by the presence of two FTIR peaks at 2866 and 2770 cm^{-1}, due to C-H bond stretching vibration. Those peaks were not present for the mSiO_2@Fe_2O_3. The presence of the organic material can be seen in the TGA graph (149 mg of C_{18} per 1 g of C_{18}@mSiO_2@Fe_2O_3), as it results in a weight loss between 220 and 700 °C. The C_{18} modification did not alter the shape of the particles and the particles

can be dispersed with a few minutes of sonication and the help of a small amount of methanol.

The mass of octadecyl groups was assessed by measuring the release of both octadecane and octadecanol from the silica by fusion in potassium hydroxide. A mass of 1.7 mg per gram of particles was found. This assessment is significantly lower than the value calculated by means of the TGA graph. Difficulties making a C_{18} monolayer may have caused problems in the "Genieser method".

The pre-concentration of PAHs from water was carried out giving a recovery above 80%. TBT could also be extracted from water with 92 % recovery.

4.8 References

[1] J.J. Kirkland, J. J. Stefano, *Journal of Chromatographic Science* **1970**, *8*, 309.

[2] N. Masque, M. Galia, R.M. Marce, F. Borrull, *Journal of Chromatography A* **1997**, *803*, 147.

[3] E. Mylchreest, R.C.Cattley, P. M. Foster, *Toxicology Science* **1998**, *43*, 47.

[4] M. T. Kelly, M. Larroque, *Journal of Chromatography A* **1999**, *841*, 177.

[5] R.C.Martinez, E.R.Gonzalo, E.H.Hernandez, F.J. S.San, M.Flores, *Journal of Chromatography A* **2002**, *950*, 157.

[6] M. A. Mottaleb, M. Z. Abedin, *Analytical Sciences* **1999**, *15*, 283.

[7] P. Silberzan, L. Leger, D. Ausserre, J. J. Benattar, *Langmuir* **1991**, *7*, 1647.

[8] A. Y. Fadeev, T. J. McCarthy, *Langmuir* **2000**, *16*, 7268.

[9] T. Hatakeyama, F. X. Quinn, *Thermal Analysis: Fundamentals and Applications, Vol. 1*, John Wiley, New York, **1994**.

[10] H.-G. Genieser, D. Gabel, B. Jastorff, *Journal of Chromatography A* **1982**, *244*, 368.

[11] R. M. Marcé, F. Borrull, *Journal of Chromatography A* **2000**, *885*, 273.

[12] H. P. Nirmaier, E. Fischer, A. Meyer, G. Henze, *Journal of Chromatography A* **1996**, *730*, 169.

[13] E. R. Brouwer, A. N. J. Hermans, H. Lingeman, U. A. T. Brinkman, *Journal of Chromatography A* **1994**, *669*, 45.

[14] E. Manoli, C. Samara, *TrAC Trends in Analytical Chemistry* **1999**, *18*, 417.

[15] F. Portet-Koltalo, K. Oukebdane, L. Robin, F. Dionnet, P. L. Desbène, *Talanta* **2007**, *71*, 1825.

Chapter 5

Overall Conclusions

5.1 Conclusions

The main purpose of this research project was to develop new solid phase materials for the extraction and pre-concentration of toxic heavy metals and organic pollutants. These materials are characterised by the presence of a superparamagnetic core surrounded by a modified mesoporous silica layer. Once these "scavengers" are dispersed in water, they can bind on their surface metal ions and organic pollutants. With a simple magnet it is possible to recover them from the solution, along with the analyte.

Silica prepared using methods based on the original Stöber procedure give low surface areas. A hexadecyltrimethylammonium chloride template was therefore used to form a mesoporous silica layer, increasing the loading of silane coupling agents and consequently their capacity to take up the analyte.

In this project dithiocarbamate and octadecyl groups were bound to the solid to tailor the materials to specific applications.

Dithiocarbamated materials were tested for the extraction of copper from waters of different pH values, but poor uptakes were achieved. Large quantities of iron were found in solution and that was a strong competitor for the surface chelating

groups, preventing analyte collection. Complete coverage and protection of the magnetic core is currently considered rather optimistic and difficult to realize in practice. Even though it was possible to reduce iron leakage, iron competition proved to be too problematic, preventing the particles extracting heavy metals from real water samples, where they are present in trace quantities.

The leakage of iron did not however affect the sorption properties of the octadecyl based particles for organic pollutants, as in this case the collection chemistry involved the affinity of non-polar C_{18} chains towards pure organic molecules and iron did not compete with the analytes in any way.

Working with these magnetic solid phase extractors, it was possible to combine the advantages of other extraction systems, such as liquid-liquid and solid phase extraction cartridges into a dispersion-partition approach.

A number of samples can be quickly treated in the field (for example at a river or lake site) in a shorter period of time. Following on site extraction and analyte recovery the weight and the volume of sample to be transported to the laboratory are minimised. The analyte, being bound to a support, is also more protected against contamination and loss.

Finally with these particles it is possible to use less solvents and electric power, so they can be considered more environmentally and economically friendly.

5.2 Further Work

This project has made a good start in developing new types of solid phase materials and further research is required to broaden the range of their applications.

- Octadecyl based particles should be tested over a wider range of organic and organometallic pollutants.

- The extraction of heavy metals may be achieved indirectly; the analyte being collected onto a C_{18} silica material in the form of an organic complex.

- A masking agent may be introduced into the sample with the aim of inhibiting iron complexation by the dithiocarbamated silica.

- The presence of iron may be avoided completely by changing the nature of the magnetic core. In this way heavy metal extraction by magnetic solid phase materials may become reliable.

- In order to increase the sorbent properties, several other modifications may be carried out on these particles. Different polymeric structures (both synthetic and artificial) can be synthesized and bound to them. Chitosan for example is a linear polysaccharide that has been proved to have sorbent properties towards metal cations and has been bound to a silica surface.

- It would be interesting to assess how contamination and loss affect accuracy over time, once the analytes had been separated from solution and bound to the magnetic support. This would help in the understanding of how long they can be safely stored between the sampling to the analysis.

- To guarantee an economic advantage, the reuse of the particles has to be an important aspect of a future project. It should be possible to use every batch of material in more than one analysis before it loses its sorbent properties.